Environmental controls of winter soil carbon dioxide fluxes in boreal and tundra environments

Alex Mavrovic[1-2-3-4], Oliver Sonnentag[2-4], Juha Lemmetyinen[5], Carolina Voigt[4-6], Nick Rutter[7], Paul Mann[7], Jean-Daniel Sylvain[8], Alexandre Roy[1-2]

[1] Université du Québec à Trois-Rivières, Trois-Rivières, Québec, G9A 5H7, Canada
[2] Centre d'Études Nordiques, Québec, Québec, G1V 0A6, Canada
[3] Polar Knowledge Canada, Canadian High Arctic Research Station campus, Cambridge Bay, Nunavut, X0B 0C0, Canada
[4] Université de Montréal, Montréal, Québec, H3T 1J4, Canada
[5] Finnish Meteorological Institute, Helsinki, FI-00560, Finland
[6] University of Eastern Finland, Kuopio, 70211, Finland
[7] Northumbria University, Newcastle upon Tyne, NE1 8ST, UK
[8] Ministère des Ressources naturelles et des Forêts, Québec, Québec, G1H 6R1, Canada

Correspondence to: Alex Mavrovic (Alex.Mavrovic@uqtr.ca)

Abstract. The carbon cycle in Arctic-boreal regions (ABR) is an important component of the planetary carbon balance, with growing concerns about the consequences of ABR warming on the global climate system. The greatest uncertainty in annual carbon dioxide (CO_2) budgets exists during winter, primarily due to challenges with data availability and limited spatial coverage in measurements. The goal of this study was to determine the main environmental controls of winter CO_2 fluxes in ABR over a latitudinal gradient (45°N to 69°N) featuring four different ecosystem types: closed-crown coniferous boreal forest, open-crown coniferous boreal forest, erect-shrub tundra, and prostrate-shrub tundra. CO_2 fluxes calculated using a snowpack diffusion gradient method ($n = 560$) ranged from 0 to 1.05 gC m^2 day^{-1}. To assess the dominant environmental controls governing CO_2 fluxes, a Random Forest machine learning approach was used. We identified soil temperature as the main control of winter CO_2 fluxes with 68% of relative model importance, except when soil liquid water occurred during zero-degree Celsius curtain conditions (i.e., $T_{soil} \approx 0°C$ and liquid water coexist with ice in soil pores). Under zero-curtain conditions, liquid water content became the main control of CO_2 fluxes with 87% of relative model importance. We observed exponential regressions between CO_2 fluxes and soil temperature in fully frozen soils (RMSE = 0.024 gC m^{-2} day^{-1}; 70.3% of mean F_{CO2}) and soils around freezing point (RMSE = 0.286 gC m^{-2} day^{-1}; 112.4% of mean F_{CO2}). F_{CO2} increases more rapidly with T_{soil} around freezing point than at $T_{soil} < 5°C$. In zero-curtain conditions, the strongest regression was found with soil liquid water content (RMSE = 0.137 gC m^{-2} day^{-1}; 49.1% of mean F_{CO2}). This study is showing the role of several variables on the spatio-temporal variability of CO_2 fluxes in ABR during winter and highlight that the complex vegetation-snow-soil interactions in northern environments must be considered when studying what drives the spatial variability of soil carbon emission during winter.

Keywords: Arctic-boreal regions, Carbon balance, Carbone dioxide flux, Random forest, Non-growing season, Winter, Soil temperature, Soil liquid water content, Snow.

1 Introduction

40 Carbon stocks and fluxes in the Arctic and boreal biomes (hereafter called Arctic-boreal regions; ABR) constitute large components of the planetary carbon balance (Tarnocai et al., 2009; van Huissteden and Dolman, 2012; Carreiras et al., 2017). ABR store substantial quantities of carbon due to inherently slow decomposition rates, largely attributable to cold temperatures (Ravn et al., 2020). ABR are warming up to four times faster than the rest of the planet with potential feedbacks to the global climate system (Derksen et

45 al., 2019; Rantanen et al., 2022). Although ongoing warming of ABR has the potential to lengthen growing seasons, enhance plant growth and increase above-ground carbon storage (Sturm et al., 2005; McMahon et al., 2010), the growing season vegetation response is variable and complex (Myers-Smith et al., 2020). Warmer air and soil temperatures enhance production and release of carbon dioxide (CO_2) from ecosystem respiration, comprising heterotrophic respiration by microbes decomposing soil organic matter, and

50 autotrophic respiration by above- and belowground plant components (Bond-Lamberty and Thomson, 2010). The release of previously frozen carbon stocks is particularly important in regions undergoing permafrost thaw (ground completely frozen for at least two consecutive years) (Schuur et al., 2015; Natali et al., 2021; Miner et al., 2022). If increases in ecosystem respiration exceed those of photosynthetic CO_2 uptake from enhanced plant growth, ABR may shift from a weak net CO_2 sink to a net CO_2 source, thereby generating a

55 potentially non-negligible, positive feedback to the global climate system (Hayes et al. 2011; Gauthier et al., 2015; Natali et al., 2019; Bruhwiler et al., 2021; Virkkala et al., 2021; Braghiere et al., 2023).

 During winter months in ABR, landscapes are generally snow-covered, photosynthesis is considered negligible, and therefore winter CO_2 fluxes derive primarily from soil respiration (Christiansen et al., 2012;

60 Webb et al., 2016). It is expected that complex soil-vegetation-snow interactions will lead to regional and local variability in soil respiration rates across ABR because of relationships between vegetation types, snow cover, soil properties, soil moisture and soil temperature (Gouttevin et al., 2012; Busseau et al., 2017; Loranty et al., 2018; Grünberg et al., 2020; Royer et al., 2021). Higher soil temperatures promote microbial activity and increase CO_2 production from soil organic matter decomposition during winter (Natali et al., 2019). A

65 snowpack acts as an important thermal insulative layer for the soil during winter, keeping soils warmer than the ambient air (Dominé et al., 2016a). Vegetation affects snow properties by increasing snow depth where wind trapping occurs (Callaghan et al., 2011a; 2011b; Busseau et al., 2017), decreasing snow density and thermal conductivity around shrubs (Gouttevin et al., 2012; Dominé et al., 2015; 2016b), decreasing albedo due to protruding branches (Ménard et al., 2012), and causing earlier spring snowmelt due to vegetation

70 thermal conductivity (Wilcox et al., 2019; Kropp et al., 2022). However, Dominé et al. (2022) showed that shrub branches within the snowpack can contribute to mid-winter soil cooling by conducting temperature through the snowpack. Hence, the complex vegetation-snow-soil interactions in northern environments must be considered when studying what drives the spatial variability of soil carbon emission during winter. Soil microbial activity can also be limited by lack or saturation of available water, meaning that higher amounts

75 of available soil liquid water (LWC) should allow higher heterotrophic respiration rates by increasing soil

microbial activity as long as the soil environment is not anaerobic (Linn and Doran, 1984; Knowles et al., 2015). Anaerobic soil conditions are usually found in fully water saturated soils.

High uncertainties in winter ABR CO_2 exchange between the ground surface and atmosphere are in part due to limited data availability because of difficulties in accessing these vast, remote regions and the harsh winter conditions creating technical challenges for CO_2 fluxes measurements (Natali et al., 2019; Virkkala et al., 2022). Methods currently available to measure wintertime CO_2 fluxes include: 1) the eddy covariance technique (Baldocchi et al., 2003), 2) chamber measurements under or above the snowpack (McDowell et al., 2000) and 3) snowpack gradient diffusion methods (Sommerfield et al., 1993). Each of these has their advantages and limitations. The eddy covariance technique (EC) exploits the atmosphere's turbulent nature to estimate net CO_2 fluxes at high temporal resolution without environmental disturbance (Baldocchi et al., 2001; Pastorello et al., 2020). Data gaps are common during the ABR winter since the EC equipment is energy-intensive and prone to failure in low temperatures. In addition, solar power supply systems are limited by low sunlight (Jentzsch et al., 2021, Pallandt et al., 2022). Furthermore, the EC equipment is stationary and cover a large footprint (250-3000 m). In contrast, plot-scale chamber techniques for measuring CO_2 fluxes are portable methods with a small footprint (< 1m) (Subke et al., 2021; Maier et al., 2022). Chambers can be used either above the snowpack or directly on the ground. Placing a chamber on the snowpack does not provide a direct measurement of soil CO_2 fluxes due to CO_2 retention and lateral diffusion within snowpacks, generally creating a negative bias and uncertainties linking the snow/atmosphere fluxes to soil fluxes (McDowell et al., 2000; Björkman et al., 2010; Webb et al., 2016). Chambers can also be placed directly on the ground by excavating the snow cover (Elberling et al., 2007), providing a direct measurement of soil CO_2 fluxes that is, however, prone to a positive bias generated by a tunnel effect due to the snow excavation (McDowell et al., 2000; Björkman et al., 2010). Unavoidable snow cover disturbance also reduces the possibility of revisiting locations for temporal surveys because the soil thermal regime is altered by the snow disturbance. Alternatively, permanent chambers can be installed before the first snowfall, but it disturbs the state of the ground and snow cover around the chamber (Webb et al., 2016). The snowpack diffusion gradient method uses snow porosity and tortuosity to estimate CO_2 fluxes from the gas concentration gradient along a vertical snow profile including ambient air above the snowpack (Sommerfield et al., 1993; Pirk et al., 2016; Kim et al., 2019). In this study, the snowpack diffusion gradient method will be used to evaluate the spatial variability of CO_2 fluxes in ABR because of its portability and minimal environmental disturbance.

The goal of this study was to determine the main environmental controls of winter CO_2 fluxes in ABR. 560 snowpack diffusion gradient measurements were made over a latitudinal gradient of four different ecosystem types common in ABR in Canada: closed-crown coniferous boreal forest, open-crown coniferous boreal forest, erect-shrub tundra and prostrate-shrub tundra. Spatio-temporal measurements of snowpack CO_2 diffusion gradients were performed at several locations in four sites during the 2020-2021 and 2021-2022 winters (December to May). Firstly, a Random Forest (RF) machine learning analysis was used to evaluate the relative importance of the following environmental variables known to exert control over winter CO_2

fluxes: soil temperature, soil LWC, vegetation type, snow water equivalent, snow depth and several snow
115   density-related measurements. Secondly, the response and uncertainty of winter CO_2 fluxes to the most
impactful environment variables determined by the RF model were quantified through regression analysis.

2 Method

2.1 Study sites

To cover different vegetation types and a wide range of soil temperature (T_{soil}) regimes and snow
120   conditions found in ABR, four study sites were selected across Canada (Fig. 1; Table 1). Each site represents
a specific ecosystem type (Royer et al., 2021), and vegetation types within each of those ecosystems were
determined using vegetation maps specific to each site. Cambridge Bay (CB), situated on the Victoria Island
in the Canadian Archipelago was the northernmost site located in the Arctic tundra dominated by lichen and
prostrate-shrub tundra. Ponomarenko et al. (2019) generated a detailed ecotype map of the Arctic tundra
125   biome present in the CB study area. Here, these ecotypes were grouped by water availability into three tundra
vegetation types from which the sampling locations (S) were selected: dry (S=94), sub-hydric (S=24) and
hydric (S=110). Trail Valley Creek (TVC), Northwest Territories, situated just north of the treeline in the
transitional zone between the boreal and Arctic biomes close to the Mackenzie delta, is dominated by erect-
shrub tundra with remaining tree patches (Martin et al., 2022). Grünberg et al. (2020) produced a vegetation
130   map of the TVC study area using airborne orthophotos, vegetation height and field observations from which
seven vegetation types and landforms were identified: lichen (S=68), tussock (S=21), dwarf shrub (S=19),
tall shrub (S=26), polygon (S=21), riparian shrub (S=17) and black spruce tree patch (S=18). Havikpak Creek
(HPC) is located just south of the treeline, at about 50 km south of TVC in an open-crown black spruce
dominated forest constituting the only type of vegetation present (S=30) (Krogh et al., 2017). Montmorency
135   Forest (MM) is the southernmost site located in a closed-crown balsam fir dominated boreal forest
constituting the only type of vegetation present (S=110) (Barry et al., 1988). The CB, TVC and HPC sites
are underlain by continuous permafrost, while the MM site is permafrost-free.
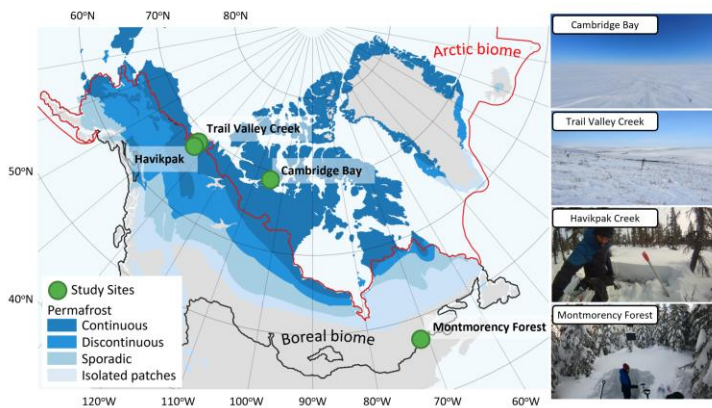
Figure 1: Study site locations in Canada. The Arctic biome is delimited following the Conservation of Arctic Flora and
140   Fauna (CAFF) working group of the Arctic Council and the boreal biome is delimited following Potapov et al. (2008).
Permafrost extent (Brown et al., 2002) is estimated in percent area: continuous (>90-100%), discontinuous (>50-90%),
sporadic (10-50%) and isolated patches (<10%).

Table 1: Study sites with the number of sampling locations in Canada and CO_2 flux measurement (N) for each site.

Site	Province/ Territory	Latitude/ Longitude	Ecosystem	Sampling locations	N	Measurement dates (YYYY-MM)	Site reference
Cambridge Bay	Nunavut	69°13'N 104°54'W	Prostrate tundra shrubs	47	230	2021-04, 15 2022-01 to 05	Ponomarenko et al., 2019
Trail Valley Creek	Northwest Territories	68°46'N 133°28'W	Erect tundra shrubs	34	190	2021-03, 04	Grünberg et al., 2020
Havikpak Creek	Northwest Territories	68°19'N 133°31'W	Open-crown coniferous boreal forest (black spruce)	5	30	2022-03	Krogh et al., 2017
Montmorency Forest	Quebec	47°18'N 71°10'W	Closed-crown coniferous boreal forest (balsam fir)	12	110	2021-01, 02, 12 2022-01 to 05	Barry et al., 1988

145

2.2 Snowpack diffusion gradient method

2.2.1 Theoretical framework for CO_2 flux calculation

During winter in ABR, soil respiration produces CO_2 below the snowpack. Consequently, a vertical CO_2 diffusion gradient is maintained through the snowpack ($d[CO_2]/dz$; gC m^{-4}), with CO_2 concentration
150 ($[CO_2]$; gC m^{-3}) decreasing with snow height from the soil surface (z; m) (Jones et al., 1999). Hereafter, $[CO_2]$ is expressed in gC m^{-3} but units of concentration could also be expressed in relative units (i.e., ppm) using the ideal gas law. The snowpack diffusion gradient method uses the $d[CO_2]/dz$ within the snowpack and Fick's first law for gas diffusion through porous media to estimate CO_2 fluxes (F_{CO2}; gC m^{-2} day^{-1}) (Sommerfeld et al., 1993; Zhu et al., 2014):

155

$$F_{CO2} = -\varphi\tau D_a \frac{d[CO_2]}{dz} \tag{1}$$

where φ represents the porosity of the snow medium, τ its tortuosity and D_a the air diffusion coefficient of the diffused gas in m^2 day^{-1}. The porosity of snow can be assessed from its density (Kinar and
160 Pomeroy, 2015):

$$\varphi = 1 - \frac{\rho_{snow}}{\rho_{ice}} + \theta \cdot \left(\frac{\rho_{water}}{\rho_{ice}} - 1\right) \tag{2}$$

where ρ represents the density of snow, water and pure ice (ρ_{ice} = -0.0001·T_{ice} + 0.9168 with T_{ice} as
165 ice temperature in °C and ρ_{ice} in g cm^{-3}; Harvey et al., 2017), and Θ is the snow liquid water content. The tortuosity is strongly correlated with porosity. Du Plessis and Masliyah (1991) established the following relationship:

$$\tau = \frac{1-(1-\varphi)^{2/3}}{\varphi} \tag{3}$$

170

Tortuosity can also be approximated as $\tau \approx \varphi^{1/3}$ (Millington, 1959; Mast et al., 1998). The d[CO_2]/dz is obtained by measuring the [CO_2] vertical profile at various snow depths. Standard air diffusion coefficients of CO_2 (unit: m^2 day^{-1}) are available in literature but must be corrected for temperature and pressure (Marrero and Mason, 1972; Massman, 1988):

175

$$D_a = 0.2020 \cdot \left(\frac{T}{T_o}\right)^{1.590} \cdot e^{-\frac{0.3738}{T/T_o}} \tag{4}$$

where T is the air temperature and T_o is the freezing point in K. The diffusion gradient method assumes that gas fluxes are the result of simple, linear, gradient-induced diffusion in uniform porosity through
180 snow cover (McDowell et al., 2000). A snowpack with strongly heterogeneous density (i.e., vertical stratification) can induce a bias when gas flow is altered by dense layers or ice crusts, typically leading to F_{CO2} overestimation (Seok et al., 2009). Such layers were rarely found in our study sites. The diffusion gradient assumption also does not hold when strong wind events occur, decreasing snowpack CO_2 concentration through wind-pumping and inducing a negative bias on CO_2 fluxes (Seok et al., 2009).
185 Consequently, d[CO_2]/dz was not measured in days following a strong wind event. Monitoring of F_{CO2} at a few sampling locations did not show any relationship between F_{CO2} and wind speed or atmospheric pressure (e.g., Fig. A1).

2.2.2 Data collection

All data were collected during the 2020-21 and 2021-22 winters between December and May (Table 1).
190 The CO_2 concentration gradient was measured by collecting gas samples at various depths in the snowpack. Each gradient profile consisted of five gas samples collected at: 1) 5 cm above the snowpack (ambient air), 2) 5 cm depth below the snowpack surface, 3) 1/3 of total snow depth, 4) 2/3 of total snow depth and 5) soil/snow interface. Gas present in snow pores was collected with a thin, hollow stainless-steel rod (50-120 cm long, 4 mm outer diameter and 2 mm inner diameter) starting with gas samples in the upper snowpack
195 and then pushing the sampling rod downward to collect gas samples deeper in the snowpack to minimize snow disturbance (Fig. 2a). Gas was collected in a 60 mL syringe (Air-Tite Luer Lock, Virginia Beach, Virginia) connected to the rod via a three-way valve. Gases were transferred into 12 mL hermetic glass vials (Labco Exetainer®, Labco Ltd., Lampeter, UK), which were sent to the Université du Québec à Trois-Rivières laboratory to be measured with a gas analyzer to obtain CO_2 concentrations. At each site, several
200 sampling locations were selected to cover the maximum range of vegetation types and snowpack characteristics, covering areas of 0.05-22.5 km^2. At each sampling location, 2 to 4 replicate profiles were measured at 50 cm spacing to test the repeatability of the sampling. A minimal spacing of 5 – 7.5 cm was required between sampling positions since it corresponds to the radius of the 60 ml sampling volume of each gas sample, based on a snow density range of 100 - 650 kg m^{-3}.

205

For typical Arctic snowpacks, samples at 1/3 depth are usually in wind slab, the dense and cohesive surface snow layer formed by strong Arctic winds. Samples at 2/3 depth are usually in depth hoar, the lower snow layer with low density and cohesion formed by a strong temperature gradient driving vertical vapor flux through the snowpack (Fig. 2b). Typically, boreal snowpacks are deeper than in Arctic tundra and display

210 a more continuous vertical stratification with increasing snow density at the bottom of the snowpack. In HPC, snowpack depths were 40-80 cm in March, while snowpack depths at MM were 100-200 cm (Fig. A2). For comparison, by March, snowpacks at CB were 10-75 cm deep and 15-150 cm at TVC.
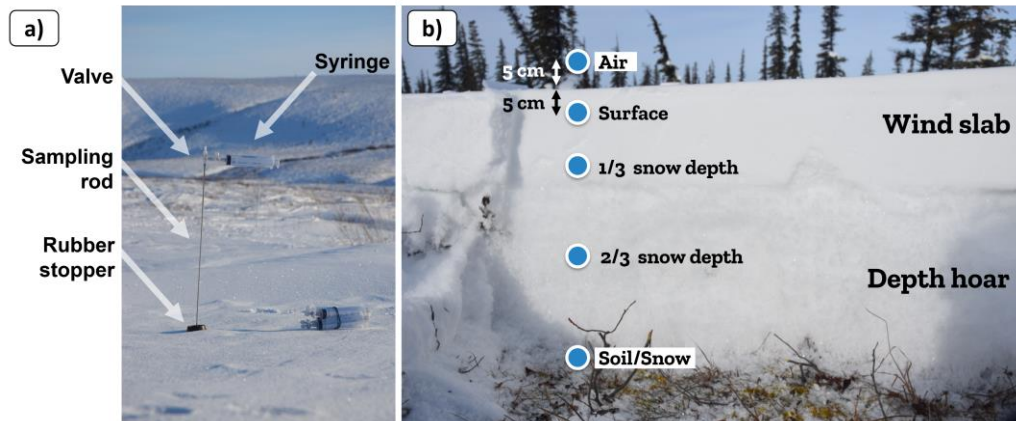
215 **Figure 2:** (a) Gas sampling equipment for the CO_2 concentration gradient measurement. (b) Typical snow depth profile of an Arctic snowpack (picture from Trail Valley Creek close to a tree patch).

Once the gas samples were collected, a vertical profile of snow and soil properties was measured to calculate the CO_2 air diffusion coefficient from the snow temperature, and snow porosity and tortuosity from

220 snow density. Snow properties were measured at every 5 cm including snow temperature (Snowmetrics digital thermometer; Fort Collins, Colorado; tenth of a degree resolution), snow density (Snowmetrics digital scale, 100 and 250 cm^3 snow cutters used to weigh snow samples; $\sigma(\rho_{snow}) \approx 9\%$; Proksch et al., 2016), snow liquid water content (hand test from Fierz et al., 2009) and snow stratigraphy. Examples of snow vertical stratification along with CO_2 concentration measurements can be found in Appendix A (Fig. A3). T_{soil} was

225 measured at 1 cm depth under the soil/snow interface as it was not possible to go deeper in frozen soil and no permanent sensors were installed (Snowmetrics digital thermometer; Fort Collins, Colorado; tenth of a degree resolution), three measurements of T_{soil} were averaged. Snow depth measurements were done with a ruler graduated every 1cm ($\sigma(d_{snow}) \approx 0.5$ cm).

230 The CO_2 concentration of 86% of gas samples were measured using a Licor LI-7810 $CH_4/CO_2/H_2O$ Trace Gas Analyzer (LI-COR Biosciences, Lincoln, Nebraska; $\sigma < 1\%$; N = 483). The gas samples were passed through an open loop along a continuous flow of a 200 ppm CO_2 calibration gas (Linde Canada, Ottawa, Ontario, Canada). Based on a calibration curve using 0, 400 and 1000 ppm CO_2 calibration gases

(Linde Canada), the CO_2 concentration of gas samples were calculated (detailed protocol: https://www.licor.com/documents/xst0ld9jozfby78bmpdqi9i7rmjjjjmg).

Randomly distributed gas samples collected during the 2020-21 winter were analyzed with a Picarro G2201-i CRDS gas analyzer (Picarro, Santa Clara, Californie; $\sigma < 0.1\%$; N = 26) to validate the method used with the LI-7810 to determine CO_2 concentration. CO_2 concentrations estimated from the LI-7810 and Picarro G2201-i gas analyzers were not significantly different in their concentration range and distribution (Fig. A4; $R^2 = 0.92$). At TVC in March 2022, a portable LI-850 CO_2/H_2O Gas Analyzer was used ($\sigma < 1.5\%$; N = 38), allowing for CO_2 concentrations to be measured on the same day as sample collection (avoiding the need for bottling and transportation). CO_2 concentrations estimated from the LI-7810 and LI-850 gas analyzers were not significantly different in their concentration range and distribution (Fig. A4b; $R^2 = 0.82$).

2.2.3 Evaluation of CO_2 flux uncertainties

An uncertainty assessment was conducted to evaluate CO_2 flux precision based on the snowpack diffusion gradient method. The uncertainty assessment focuses on random errors, as systematic errors are discussed at the end of Sect. 2.2.1. From sampling to flux estimation, several steps could add uncertainty to the results. Uncertainties can be subdivided into four sources: gas concentration estimates, gas transfer/transport/storage, evaluation of the snowpack $d[CO_2]/dz$ and snowpit measurements (i.e., snow density and temperature). Gas concentration uncertainties were evaluated from the gas analyzer precision as assessed by the manufacturer and tested using calibration gases. Six CO_2 reference gases of 400 ppm were bottled during two different field campaigns and were processed among the gas samples from the snowpack to ensure the transfer, transport and storage protocol did not lead to sample contamination. The $d[CO_2]/dz$ uncertainties were evaluated with the standard deviation from the coefficient of determination ($\sigma = \sqrt{(1 - R^2)/(N - 1)}$; Bowley, 1928). F_{CO_2} uncertainty was estimated by propagation of the uncertainties of $d[CO_2]/dz$ and snow density using Eq. 1 (Taylor, 1997). The uncertainty of ρ_{snow} was fixed at 9% (Proksch et al., 2016) while the uncertainty of $d[CO_2]/dz$ was estimated based on the root mean squared error of the linear regression for each snowpack concentration gradient measurement.

2.3 Soil volumetric liquid water content at Montmorency Forest site

Zero-degree Celsius curtain conditions exist when the soil temperature is around freezing point (0°C) and a mix of ice and liquid water coexist in the soil pore space because the phase transition between water and ice is slowed due to latent heat (Outcalt et al., 1990). Hence, liquid water content (LWC; m^3/m^3) and ice fractions can be used as a freezing/thawing indicator during the zero-curtain period. The MM study sites were equipped with TEROS 12 Soil Moisture Sensors (METER Group) at 5 cm depth. LWC was only monitored at the MM site since it was the only site where T_{soil} in upper layers remained around 0°C for the whole winter, allowing the presence of liquid water in the soil throughout winter. The Zhang et al. (2010) empirical soil liquid water and ice mixing model was used to calculate soil liquid water content (m_{uw}) (Eq. 5

to 8). LWC was estimated to be negligible at the CB, TVC and HPC sites since T_{soil} was in-between -5°C and -25°C. The model from Zhang et al. (2010) supports that at T_{soil} colder than -5°C, LWC is negligible.

$$LWC = a \cdot \frac{\rho_b}{\rho_w} \cdot |T_{soil}|^{-b} \tag{5}$$

$$\ln a = 0.5519 \cdot \ln SSA + 0.2618 \quad ; \quad \ln b = -0.264 \cdot \ln SSA + 0.3711 \tag{6}$$

where ρ_w and ρ_b (g cm^{-3}) represent liquid water and soil bulk density respectively, T_{soil} (°C) represents soil temperature, SSA (m^{-1}) represents soil particles specific surface area described by Fooladman (2011).

$$SAA = 3.89 \cdot d_g^{-0.905} \tag{7}$$

$$\ln d_g = f_c \cdot \ln M_c + f_{si} \cdot \ln M_{si} + f_{sa} \cdot \ln M_{sa} \tag{8}$$

where d_g represents the soil geometric mean particle-size diameter (mm), f and M represent soil components fraction and mean particle-size diameter (mm). Soil components are clay ($M_c = 0.001$ mm), silt ($M_{si} = 0.026$ mm) and sand ($M_{sa} = 1.025$ mm). Soil bulk density and gravimetry was evaluated using a soil sampling protocol similar to the National Forest inventory protocol (CFI, 2008). Undisturbed soil samples were collected in three homogenous horizons of a soil profile using 400 cm^2 cores. Volumetric soil samples were dried (103°C) and weighted to determine bulk density. Gravimetric samples were used to determine sand (%, 50-2000 μm), silt (%, 2-50 μm), clay (%, < 2 μm) and organic content (g/kg). The soil texture was determined by the hydrometer method (Bouyoucos, 1962), whereas the organic content was determined with a LECO organic analysis instrument (LECO corporation, Saint-Joseph, Michigan).

2.4 Random Forest algorithm

Random forest (RF) is an ensemble machine learning method based on a multitude of decision trees (Breiman, 2001). Each decision tree of our RF model (scikit-learn 1.2.1 library from python 3.10.3) is trained on a random subset of environmental variables drawn from the dataset input: T_{soil}, LWC, vegetation type, snow water equivalent, snow depth, snow mean density, snow maximum density, snow porosity, snow tortuosity, wind slab thickness (if present) and wind slab fraction relative to total snow depth (if present). Each decision tree generates a F_{CO2} prediction, and the overall RF prediction is the average of all prediction trees. A strength of the RF algorithm is that it performs well even when input variables are correlated with each other (Liaw and Wiener, 2002; Strobl et al., 2008; Kibtia et al., 2020). Our RF model was composed of 500 fully decomposed decision trees. Our dataset was randomly divided into a training subset (75%) and a testing subset (25%), preserving the relative distribution between vegetation types. Our RF model performance was assessed using the coefficient of determination (R^2), explained variance, and mean absolute error. We used our RF model to identify the relative importance of winter CO_2 flux predictors. Relative

importance of each environmental variable was computed with the permutation method, i.e., alternatively removing variables from the RF model and evaluating the performance decrease which was, measured via the coefficient of determination.

3 Results

3.1 CO_2 flux uncertainties

Evaluation of F_{CO2} precision showed that the two main sources of uncertainty are associated with snow density measurements, in agreement with Sommerfeld et al. (1996), and with $d[CO_2]/dz$ linear regression (mean $R^2 = 0.790$ ($\sigma = 0.236$) for $F_{CO2} \geq 0.01$ gC m^{-2} day^{-1}; N = 398) (Table A1). Snow density uncertainty ($\sigma(\rho_{snow}) \approx 9\%$) impacted snow porosity and tortuosity in Eq. 1. From the linear fit of Fig. 3, the average F_{CO2} uncertainty can be estimated at 19.4%, which provides sufficient accuracy to observe the impact of environmental variables on winter F_{CO2}.
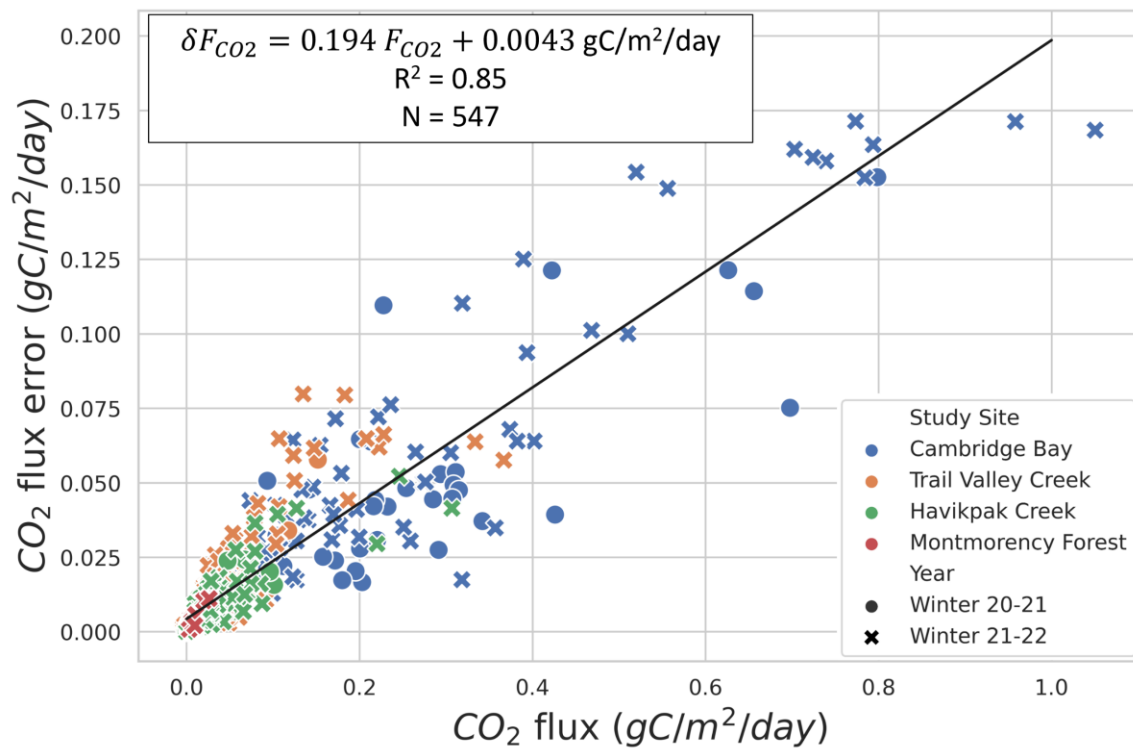
Figure 3: CO_2 flux (F_{CO2}) uncertainty relationship to F_{CO2} for four study sites and two winters 2020-2021 and 2021-2022. Specifications of the linear fit can be found in the upper left. The data dots color indicates the study site and its symbol (i.e., circle or x-shaped) indicates the winter during which it was collected.

The overall $[CO_2]$ precision of around 1% shows that the measurement technique is not a main source of uncertainty in F_{CO2} estimates. Gas concentration estimations from LI-7810 have a precision of 0.88% at 400 ppm according to the manufacturer. The stability of the $[CO_2]$ measurement was evaluated over 169 measurements displaying a standard deviation of 0.09%. The LI-7810 was further tested using a 400

ppm calibration gas with a 1% [CO_2] precision (Linde Canada). A linear calibration fit equation was used to estimate [CO2] of small gas samples, using 3 calibration gases (200, 400, 1000 ppm) plus the theoretical zero intercept. Average uncertainty of the linear regression was 0.76% over six calibration runs with a standard deviation of 0.15%. The average accuracy of the reference [CO_2] bottled among the gas samples from the snowpack was 1.11%.

3.2 Spatio-temporal variability of winter CO₂ fluxes associated with abiotic controls

The RF model determined T_{soil} and LWC to be the two main predictors of winter CO_2 fluxes. We found two temperature and LWC regimes of winter F_{CO2} (Fig. 4). The first regime was when the soil was frozen with $T_{soil} < 0^{\circ}C$ and LWC < 0.2 m^3/m^3 leading to F_{CO2} being mainly controlled by T_{soil}. The second regime was when LWC > 0.2 m^3/m^3 and < 0.42 m^3/m^3 but with a fraction of it's water in the form of ice (zero curtain condition), causing LWC to be the main control of F_{CO2} instead of T_{soil}. While the first regime mostly corresponds to Arctic study sites, the second regime only includes one study site (MM) located in the southern boreal forest. Therefore, conclusions from the second regime should be less generalized than those from the first regime. Subsequent evaluation focused on the response of winter CO_2 fluxes to T_{soil} and LWC using exponential regressions in order to better understand the role of these two variables on winter CO_2 fluxes.

3.2.1 Variable importance determined by Random Forest model

T_{soil} was the F_{CO2} predictor with the highest relative importance (68%) when using the complete dataset (Fig. 4a), followed by LWC (17%). Snowpack characteristics, ρ_{snow} (11%) and snow water equivalent (SWE) (2%), had a lower relative importance in the RF model. Contrary to what might be expected, the vegetation type had near-negligible relative importance (1%) in F_{CO2} prediction. The RF model was developed starting with all environmental variables available: T_{soil}, LWC, vegetation type, SWE, snow depth, mean ρ_{snow}, max ρ_{snow}, φ, τ, wind slab fraction and wind slab thickness. Although the correlation of several snow parameters did not decrease the RF model performance, snow parameters impacted the assessment of variable relative importance by splitting the relative importance between the correlated variables. Consequently, variables with lower importance and with no significant impacts on the RF performance were progressively removed. The two selected snow parameters that had significant impact were SWE and ρ_{snow}. MM was the only site where soil LWC was present, enabling the assessment of the relative importance of this variable. When using only data from MM in the RF model (Fig. 4b), the relative importance of T_{soil} (12%) on F_{CO2} was lower than with all combined datasets since T_{soil} was near 0°C for all measurements. At MM, LWC becomes the main predictor (87%) of F_{CO2}, while ρ_{snow} importance drops (2%) and SWE remains similar (< 1%).
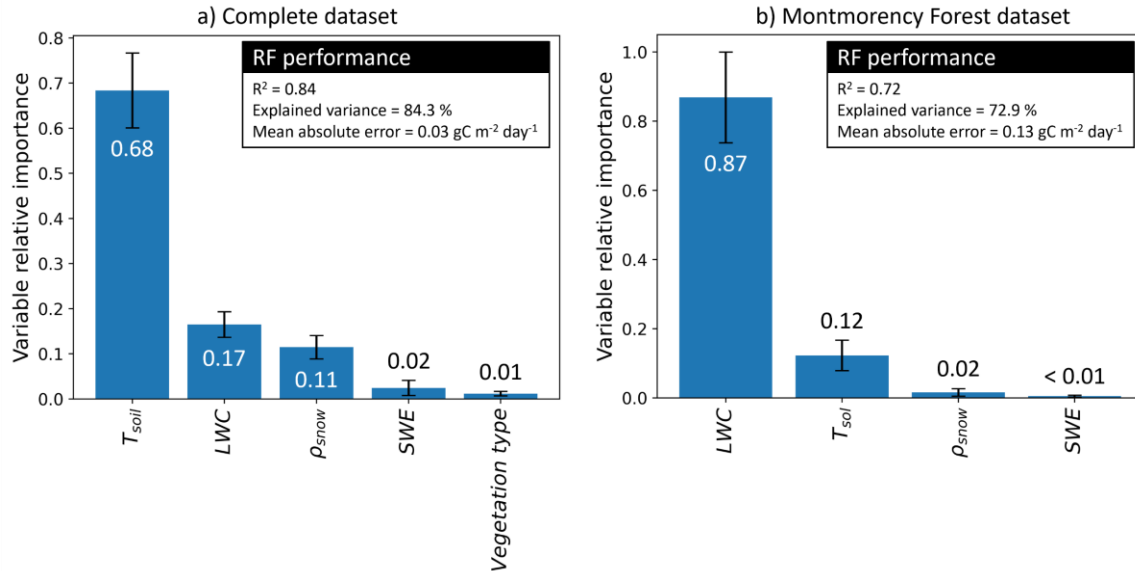
Figure 4: Random Forest (RF) performance and variable relative importance. Variables used are soil temperature (T_{soil}), soil liquid water content (LWC), snow density (ρ_{snow}), snow water equivalent (SWE) and vegetation type. (a) The first iteration integrated the complete dataset and (b) the second iteration only integrated Montmorency Forest dataset with LWC > 0 m^3 m^{-3}. The values displayed by the bar plot is the mean variable relative importance over 100 permutations, while the error bars are the standard deviation.

3.2.2 Soil temperature

Figures 5 and 6 show the relationship between winter F_{CO2} and T_{soil}. Figure 5 focuses on T_{soil} < 0°C from CB, TVC, HPC and MM. An exponential regression was used to evaluate the relationship between T_{soil} and F_{CO2} estimates (RMSE = 0.024 gC m^{-2} day^{-1}). F_{CO2} at MM when T_{soil} < 0°C and LWC < 0.2 m^3/m^3 were included in this graph because they are more strongly correlated to T_{soil} than LWC (see Sect. 3.2.3). Note that the low number of F_{CO2} measurements with T_{soil} between -6°C to -0.5°C restrict the capacity to evaluate the regression within this range. Using the exponential regression of Natali et al. (2019), we obtained a RMSE of 0.030 gC m^{-2} day^{-1}. The regression of Natali et al. (2019) generally shows an overestimation of fluxes for T_{soil} < -5°C, but an underestimation for T_{soil} > 5°C when compared to our exponential regression. The systematic bias between our dataset and the regression of Natali et al. (2019) is minimal (mean bias = -0.0025 gC day^{-1} m^{-2}). We also observed the isolated occurrence of comparably large winter F_{CO2} up to 0.36 gC m^{-2} day^{-1} at temperatures below -10°C (Fig. 5). These measurements of high F_{CO2} at low temperature seems to be genuine since the repeatability was verified over the 3 sampling profiles performed at each site. Nevertheless, we were not able to explain these strong F_{CO2} fluxes and no environmental variables measured in our study could be linked to those occurrences. It has been suggested that gas bursts during autumn freeze-up in permafrost environments might be due to gas compression by ice formation and ground cracking (Pirk et al. 2015). This hypothesis can be considered to explain the high F_{CO2} observed in this study, although the high F_{CO2} observed occurred at a near-surface T_{soil} between -25°C and -10°C so the freeze-up would have to occur at lower depths in the soil. Figure 6 displays the higher winter F_{CO2} from MM where T_{air} are higher and the important snowpack insulation keeps the soil at temperatures around 0°C through the entire winter. F_{CO2} increases more rapidly with T_{soil} around freezing point than at T_{soil} < 5°C, which is shown by the higher temperature-

dependency parameter (B = 2.82 °C^{-1}) of the MM site exponential regression (RMSE = 0.286 gC m^{-2} day^{-1}) compared to the exponential regression of Fig. 5 (B = 0.18 °C^{-1}). This discrepancy in temperature-dependency

385   creates a discontinuity between the measurements at $T_{soil} < 5°C$ and $T_{soil} \approx 0°C$ that did not allow for a continuous temperature-dependency regression across all the study sites. The lower RMSE of the exponential regression of Fig. 5 (RMSE = 0.024 gC m^{-2} day^{-1}; 70.3% of mean F_{CO2}) compared to the exponential regression of the MM site (RMSE = 0.286 gC m^{-2} day^{-1}; 112.4% of mean F_{CO2}) might be due to the impact of soil LWC at the MM site (see Sect. 3.2.3).

390
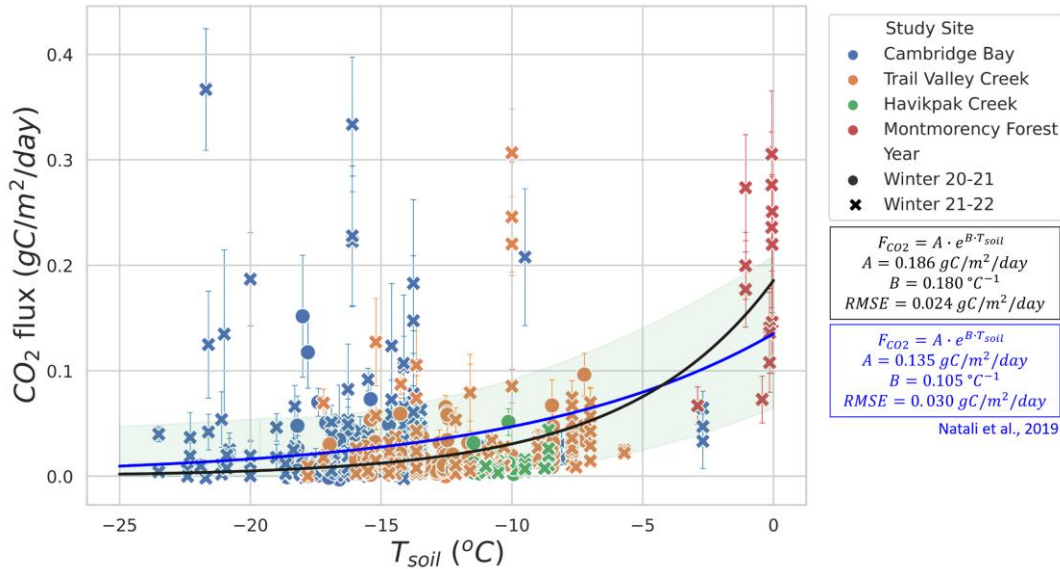
Figure 5: CO_2 flux (F_{CO2}) as a function of surface soil temperature (T_{soil}) for $T_{soil} < 0°C$. An exponential regression was fitted with the data (black line) and compared to the exponential regression by Natali et al. 2019 from an external dataset (blue line).
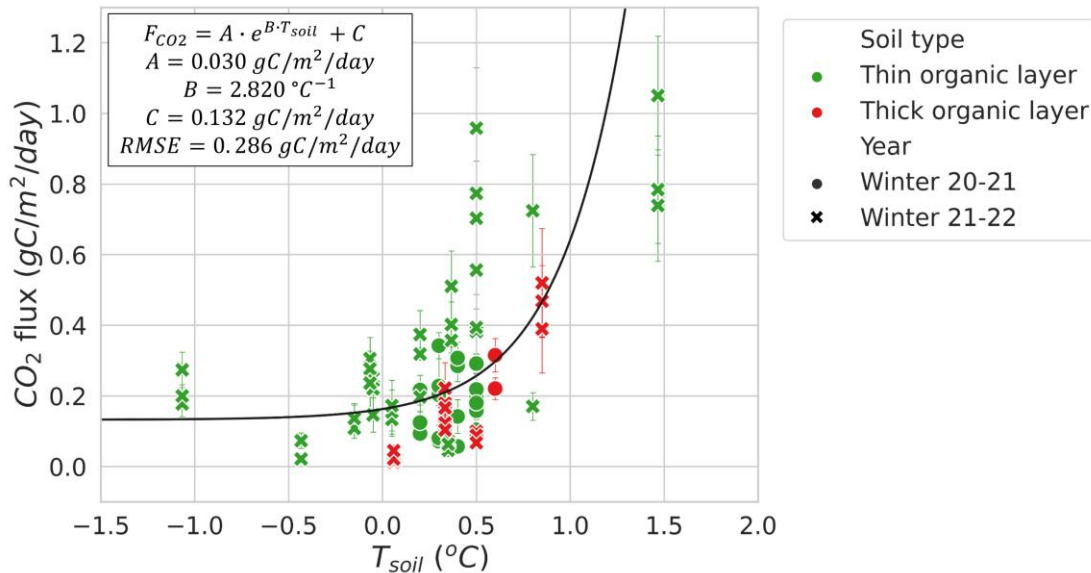
395

Figure 6: CO_2 flux (F_{CO2}) as a function of soil temperature (T_{soil}) at the Montmorency Forest study sites where soil liquid water content (LWC) was greater than 0 m^3/m^3 throughout winter. An exponential regression was fitted to the data (black line).

3.2.3 Soil liquid water content

400   The relationship between LWC and F_{CO2} during winter at MM (RMSE = 0.137 gC m^{-2} day^{-1}; 49.1% of mean F_{CO2}) was stronger than between T_{soil} and F_{CO2} (RMSE = 0.286 gC m^{-2} day^{-1}; 112.4% of mean F_{CO2}), when excluding the sampling location that contained a thick organic soil layer with very high soil moisture due to its location near the bottom of a microtopographic depression (Fig. 7). Other MM sampling locations with a thin organic layer shared a similar soil composition dominated by mineral soils. The strong correlation

405   between LWC and F_{CO2} was mostly observed at LWC > 0.2 m^3/m^3 and < 0.42 m^3/m^3. The plateau observed in Fig. 7 indicates that T_{soil} might be a better predictor than LWC at LWC < 0.2 m^3/m^3.
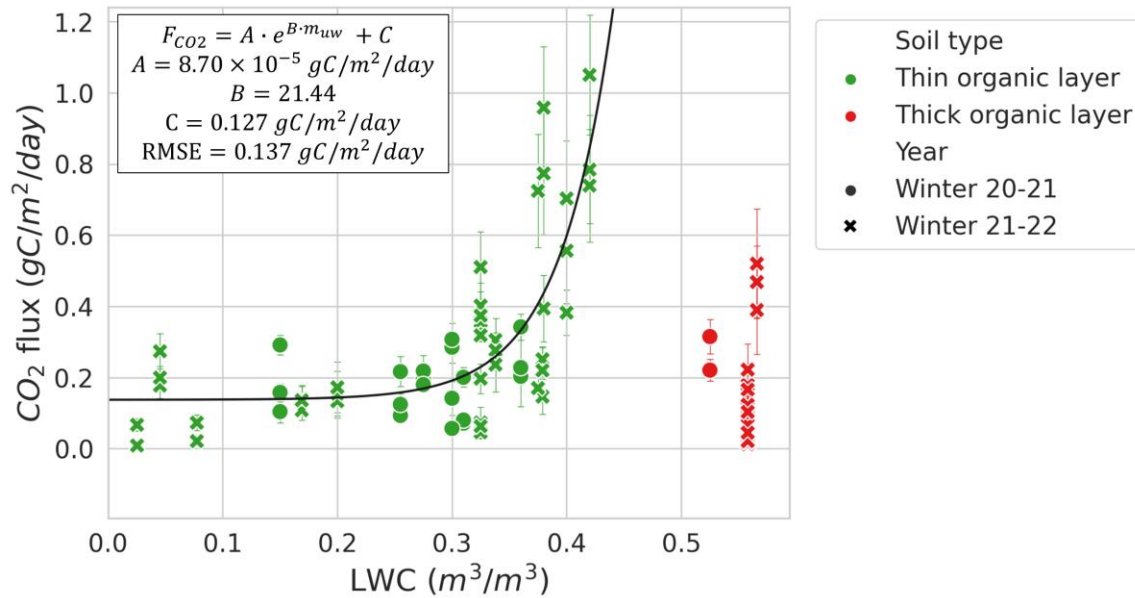
Figure 7: CO$_2$ flux (F_{CO2}) as a function of soil volumetric liquid water content (LWC) at the Montmorency Forest study
410   site. An exponential regression was fitted to the data (black line), excluding the thick organic layer site (red markers).

3.2.4 Vegetation types

Figure 8 shows winter F_{CO2} across the four study sites for different vegetation types. Since CB vegetation is mostly prostrate-shrub tundra, CB ecosystems were regrouped by water availability. In average, higher winter F_{CO2} at CB were observed in environments experiencing wetter conditions during the growing

415   season. At TVC, several vegetation and land cover types are present. F_{CO2} from MM were higher than for the other sites. Higher F_{CO2} can be explained by warmer mean annual average temperature, a deeper snowpack and winter T_{soil} around 0°C (See Sect. 3.4).

Vegetation type was not identified as a strong predictor of F_{CO2} by the RF model. Nonetheless, we

420   observed differences in the mean and range of F_{CO2} for the various vegetation types probed in this study. This might be due to the strong correlation between vegetation type and soil temperature (Fig. A5), as well as relationships between vegetation and soil type, including soil organic matter content and soil pore size. The RF algorithm showed vegetation type relative importance increased to 42% when T_{soil} was removed from the

environmental variables, although the removal of T_{soil} decreased RF performance substantially ($R^2 = 0.40$).

425 Therefore, vegetation could be used as a proxy variable for T_{soil} if the latter is not available to predict F_{CO2}, but with poorer results.
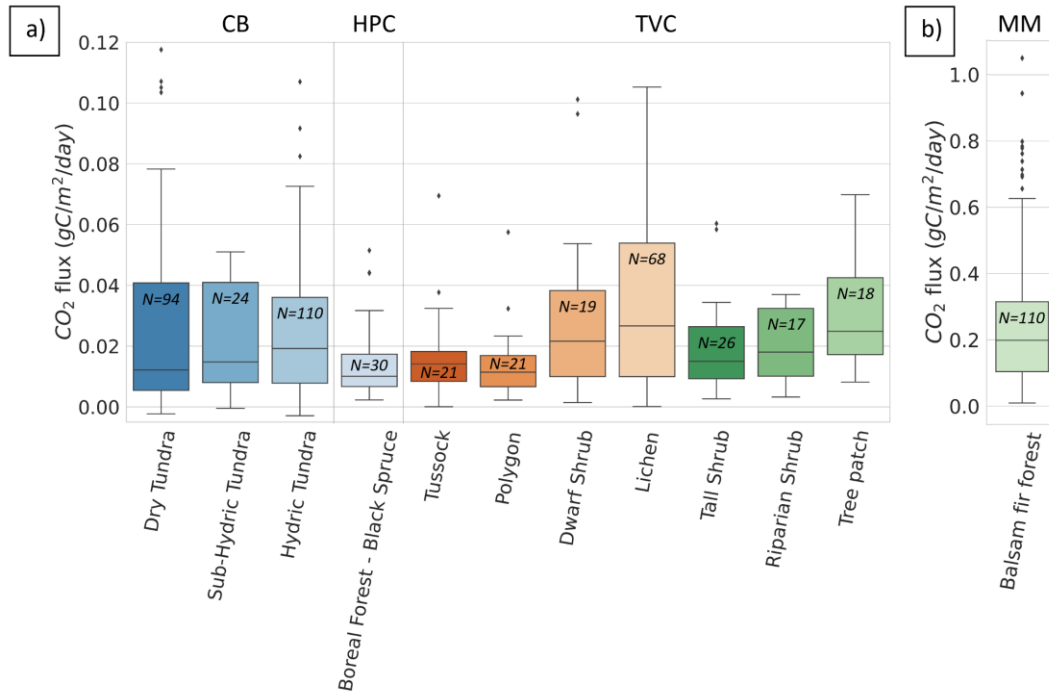
Figure 8: Boxplot of CO_2 flux (F_{CO2}) across 12 vegetation types and 4 sites. F_{CO2} from Montmorency Forest (MM) are
430 on a separate scale because they are much higher than the colder environments (b). Cambridge Bay (CB) sites are ordered by increasing water availability and Trail Valley Creek (TVC) sites are ordered by increasing mean soil surface temperature in March 2021 and 2022. Havikpak Creek (HPC) and MM were composed of a single vegetation type. Outliers were defined as $F_{CO2} > Q3 + 1.5$ IQR where Q3 is the third quartile and IQR the interquartile range. Outliers are out of y-axis range for the dry tundra (4), sub-hydric tundra (4), hydric tundra (4) and lichen (3). The outliers can be
435 found in Fig. 5.

4 Discussion

4.1 Controls of winter CO₂ fluxes

The RF model predictors' relative importance showed that during winter, T_{soil} emerged as the dominant predictor of F_{CO2} when the soil was frozen. Nevertheless, in the closed-boreal forest site (i.e., MM) where
440 zero-curtain conditions persisted throughout winter, soil LWC took precedence as the dominant predictor as there was minimal variation in T_{soil} under these conditions. Our results confirm the strong winter F_{CO2} dependency on T_{soil} shown by Natali et al. (2019), although we observed fluxes lower than reported by Natali et al. (2019) at $T_{soil} < -5°C$ and mostly higher fluxes at $T_{soil} > -5°C$. Considering the two regressions of the relationship between T_{soil} and F_{CO2} have large uncertainties attached to them, the difference between them
445 falls inside the uncertainty margin (Fig. 5). It should be noted that the Natali et al. (2019) regression was obtained using F_{CO2} estimates from several methods including eddy covariance, chamber and snowpack

diffusion measurements, whereas our study exclusively uses the latter. Several studies have shown bias between the different measurement methods; eddy covariance and soil chamber methods displayed positive biases when compared to snowpack diffusion measurements (McDowell et al., 2000; Björkman et al., 2010; Webb et al., 2016), while the snow chamber displayed negative biases when compared to the snowpack diffusion measurements (McDowell et al., 2000). It should be reminded that the T_{soil} used in his study refers to near-surface temperature, deeper T_{soil} may vary and affect the correlation with F_{CO2}.

4.2 Zero-curtain conditions

Soil LWC was observed only at the MM site, where T_{soil} was around 0°C throughout winter. In zero-curtain conditions, LWC was shown to become the dominant control of winter F_{CO2}, while T_{soil} importance diminished. It should be noted that it would be ill-advised to generalize the relationship between soil LWC and F_{CO2} as it is only based on data from one study site, and it cannot be ruled out that this relationship is site-specific depending on soil and vegetation composition. Nevertheless, our study highlighted the important impact of LWC on F_{CO2} around soil freezing point when there is a mixed state of ice and free water in soils. When the soil is at zero-curtain, the latent heat governs the ice and liquid water ratio in the soil (Devoie et al., 2022). Hence, LWC and ice fractions can be used as a freezing/thawing indicator during the zero-curtain period and help better quantify the F_{CO2} fluxes in boreal forest environments where zero-curtain conditions prevail (Prince et al., 2019). This result is particularly important in ABR since the duration and frequency of zero-curtain periods are expected to increase in a warming climate (Yi et al., 2015 and 2019, Tao et al., 2021). Further research on winter F_{CO2} in zero-curtain conditions should investigate different sites to assess if the relationship between F_{CO2} and soil LWC is site-specific or dependent on soil properties. It should be noted that one of the measurement locations at MM displayed low F_{CO2} despite its LWC being the highest of all sites. The soil composition of this site consisted of a thick (> 30 cm) soil organic top layer, whereas all other measurements were done at sites with thinner (3-10 cm) organic layers on top of mineral soil. It is well known that anaerobic conditions created by high soil moisture (at least > 50%) constrain soil CO_2 respiration rates during the growing season because many microorganisms require oxygen for organic matter decomposition which they lack if soil pores are filled with water (Linn and Doran, 1984; Davidson and Janssens, 2006).

4.3 Snowpack importance

Our study shows that abiotic variables related to T_{soil}, LWC, and physical snowpack properties explain the majority of variance in winter CO_2 fluxes. It should be noted that we did not incorporate variables related to temporal dynamics such as the previous days' soil temperature and LWC, which have been shown by Harel et al. (2023) to be of importance during the growing season. However, winter soil variables are not expected to be as dynamic as during the growing season because of the snowpack insulating properties. The RF model showed that SWE and mean snow density were the snow characteristics that provided the greatest improvement of the RF model, although to a lesser degree than T_{soil} and LWC. The importance of snow characteristics in F_{CO2} is linked with the strong correlation to T_{soil} (Dominé et al., 2016a; Pedron et al., 2023),

although a snapshot of snow conditions provides limited abilities to infer T_{soil} as shown in Slater et al. (2017). Snow properties temporal information is required to predict the impact of snow insulation on T_{soil}, with the most important period being in the autumn freeze-up when air temperature decreases below the freezing

485 point. Snow characteristics are closely linked to topography (Meloche et al., 2021), and thus soil wetness and soil carbon content (Gouttevin et al., 2012). Regarding the snowpack diffusion gradient method, the snowpack is used to estimate winter CO_2 fluxes. An average snow density was used to estimate snow porosity and tortuosity used in CO_2 flux calculations (Eq. 1), which does not consider the vertical stratification of the snowpack. However, the diffusion gradient remained linear despite vertical stratification in snow density

490 (e.g., Fig. A3 where the average ratio between the standard deviation and mean of $D_{air} \cdot \varphi \cdot \tau$ is around 10%) which points toward a minimal impact of this assumption on our results.

4.4 Soil biogeochemistry

The unexplained variance (16%) suggests that winter CO_2 fluxes might have been controlled by other environmental variables such as soil physical-chemical properties regulating soil biogeochemistry and soil

495 redox conditions, which were neither addressed nor measured in this study. CO_2 production is governed by the availability and quality of labile C compounds regulating the decomposition of soil organic matter (Michaelson et al., 2005; Wang et al., 2011), and the activity and composition of the soil microbial community (Monson et al., 2006). Soil type and structure, for example the thickness of the organic layer, soil pore size distribution, as well as soil pH may be further strong controls on CO_2 production (Steponavičienė

500 et al., 2022; Yli-Halla et al., 2022). All these variables vary widely across the heterogeneous tundra terrain (Virtanen and Ek, 2014), where small-scale moisture, vegetation and soil conditions occur among hummock and inter-hummock depressions (Wilcox et al. 2019). Further analysis is required to understand the role of physical-chemistry soil properties on F_{CO2} during winter.

4.5 Relevance for terrestrial biosphere models

505 Large uncertainties remain in terrestrial biosphere models used to estimate CO_2 fluxes in the ABR (Fisher et al., 2014; Tei and Sugimoto, 2020; Birch et al., 2021; Virkkala et al., 2021), especially regarding the respiratory release of CO_2 via soil respiration (the sum of heterotrophic respiration and belowground autotrophic respiration) during winter (Natali et al., 2019). The limited number of observational data available has restricted model improvements, testing, and evaluation (Virkkala et al., 2022). Modelling the ABR carbon

510 cycle is critical for climate projections since a warmer climate should lead to higher T_{soil}, thus increasing ABR winter F_{CO2} (Mellander et al., 2007; Throop et al., 2012; Wieder et al., 2019). Several terrestrial biosphere models are currently in use (Fisher et al., 2022), such as CLM (Community Land Model; Lawrence et al., 2019) and CLASSIC (Canadian Land Surface Scheme Including Biogeochemical Cycles; Melton et al., 2020; Seiler et al., 2021). The F_{CO2} relationships to T_{soil} and LWC observed in this study could be used

515 to inform terrestrial biosphere models through the parametrization of winter soil respiration sensitivity to soil temperature (e.g., Q10) and LWC in zero-curtain conditions. Our study shows that permanent installation of

the snow gradient method (Seok et al., 2009; Zhu et al., 2014; Graham and Risk, 2018) would be suitable to gather temporal non growing season CO_2 fluxes in ABR required to fully test terrestrial biospheres models.

5 Conclusion

520   Our study showed that T_{soil} is the main control of winter F_{CO2} at $T_{soil} < 0^oC$ in ABR. The relative importance analysis of our RF model showed that T_{soil} was the main predictor of F_{CO2}, followed by LWC. However, we found that at our site maintaining zero-curtain conditions throughout winter, LWC becomes the main control of winter F_{CO2}. We observed non-negligible winter F_{CO2} that may partially offset growing season CO_2 uptake in ABR. Consequently, winter F_{CO2} must be properly estimated in terrestrial biosphere

525   models and climate models. Additionally, future research should focus on linking the effects of abiotic variables on F_{CO2} during winter, as we determined here, with soil biogeochemistry, microbial functioning and vegetation.

6 Acknowledgements

This work was made possible thanks to the contributions of the Natural Sciences and Engineering Research

530   Council of Canada (NSERC), the Fonds de recherche du Québec – Nature et technologies (FRQNT) and Polar Knowledge Canada (POLAR). A special thanks to everybody that contributed to data collection and gas analyzing: Elise Imbeau (Viventem), Gabriel Ferland (Viventem), Aili Pedersen (POLAR), Gabriel Hould Gosselin (Université de Montréal [UdeM] and Wilfrid Laurier University [WLU]), Emma Riley (WLU), Rosy Tutton (WLU), Victoria Dutch (Northumbria University [NU]), Georgina Woolley (NU), Élise

535   Groulx (Université de Sherbrooke [UdeS]), Charlotte Crevier (UdeS), Érika Boisvert (UdeS), Alain Royer (UdeS), Patrick Ménard (UdeS), Vincent Sasseville (UdeS), Célia Trunz (UdeS), Daniel Kramer (UdeS), Estéban Hamel Jomphe (UQTR), Samuel Goulet (UQTR), Alex Gélinas (UQTR), David de Courville (UQTR), Juliette Ortet (UQTR) and Chris Derksen (Environment and Climate Change Canada). We would also like to thank Ian Hogg, Johann Wagner and Scott Johnson from POLAR for their logistical support.

540   ## 7 Competing interests

The authors declare that they have no conflict of interest.

8 Data availability

Mavrovic, A., Sonnentag, O., Voigt, C., Roy, A. (2023). Winter CO2 fluxes over arctic and boreal environments. Borealis, V1, UNF:6:u35JsrWpGNJSM3chSR9Ssg== [fileUNF]. doi:

545   10.5683/SP3/R3KZEQ

References

Baldocchi, D., Falge, E., Gu, L., Olson, R., Hollinger, D., Running, S., Anthoni, P., Bernhofer, C., Davis, K., Evans, R.,
550   Fuentes, J., Goldstein, A., Katul, G., Law, B., Lee, X., Malhi, Y., Meyers, T., Munger, W., Oechel, W., Paw
U, K., Pilegaard, K., Schmid, H., Valentini, R., Verma, S., Vesala, T., Wilson, K., and Wofsy, S.: FLUXNET:
A New Tool to Study the Temporal and Spatial Variability of Ecosystem–Scale Carbon Dioxide, Water Vapor,
and Energy Flux Densities. Bull. Am. Meteorol., 82(11), 2415–2434, doi: 10.1175/1520-
0477(2001)082<2415:fantts>2.3.co;2, 2001.

555

Baldocchi, D.: Assessing the eddy covariance technique for evaluatingcarbon dioxide exchange rates of ecosystems :
past, presentand future. Glob. Chang. Biol., 9(4), 479-492, doi: 10.1046/j.1365-2486.2003.00629.x, 2003.

Barry R, Plamondon, AP, and Stein, J.: Hydrologic soil properties and application of a soil moisture model in a balsam
560   fir forest. Can. J. For. Res., 18(4), 427– 434, doi: 10.1139/x88-063, 1988.

Birch, L., Schwalm, C., Natali, S., Lombardozzi, D., Keppel-Aleks, G., Watts, J., Lin, X., Zona, D., Oechel, W., Sachs,
T., Black, T. A., and Rogers, B.: Addressing biases in Arctic–boreal carbon cycling in the Community Land
Model Version 5. Geosci. Model Dev. Discuss., 14, 3361-3382, doi: 10.5194/gmd-14-3361-2021, 2021.

565

Björkman, M., Morgner, E., Cooper, E., Elberling, B., Klemedtsson, L., and Björk, R.: Winter carbon dioxide effluxes
from Arctic ecosystems : An overview and comparison of methodologies. Glob. Biogeochem. Cycles, 24,
GB3010, doi: 10.1029/2009GB003667, 2010.

570   Bond-Lamberty, B., and Thomson, A.: Temperature-associated increases in the global soil respiration record. Nature,
464, 579–582, doi:10.1038/nature08930, 2010.

Bouyoucos, G.J.: Hydrometer Method Improved for Making Particle Size Analyses of Soils. Agron. J., 54(5), 464–465,
doi: 10.2134/ agronj1962.00021962005400050028x, 1962.

575

Bowley, A.: The Standard Deviation of the Correlation Coefficient. J. Am. Stat. Assoc., 23(161), 31–34,
doi:10.2307/2277400, 1928.

Braghiere, R., Fisher, J., Miner, K., Miller, C., Worden, J., Schimel, D., and Frankenberg, C.: Tipping point in North
580   American Arctic-Boreal carbon sink persists in new generation Earth system models despite reduced
uncertainty. Environ. Res. Lett,. 18(2), 025008, doi: 10.1088/1748-9326/acb226, 2023

Breiman, L.: Random forests. Mach. Learn., 45, 5-32, doi: 10.1023/A:1010933404324, 2001.

585   Brown, J., Ferrians, O., Heginbottom, J., and Melnikov, E.: Circum-Arctic Map of Permafrost and Ground-Ice
Conditions, Version 2. Boulder, Colorado USA. NSIDC: National Snow and Ice Data Center, doi:
10.7265/skbg-kf16, 2002.

590   Bruhwiler, L., Parmentier, F.-J., Crill, P., Leonard, M., and Palmer, P.: The Arctic Carbon Cycle and Its Response to Changing Climate. Curr. Clim. Change Rep., 7, 14-34, doi: 10.1007/s40641-020-00169-5, 2021.

Busseau, B.-C., Royer, A., Roy, A., Langlois, A., and Dominé, F.: Analysis of snow-vegetation interactions in the low Arctic-Subarctic transition zone (northeastern Canada). Phys. Geogr., 38(2), 159-175, doi: 0.1080/02723646.2017.1283477, 2017.

595

Callaghan, T., Johansson, M., Brown, R., Groisman, P., Labba, N., Radionov, V., Bradley, R., Blangy, S., Bulygina, O., Christensen, T., Colman, J., Essery, R., Forbes, B., Forchhammer, M., Golubev, V., Honrath, R., Juday, G., Meshcherskaya, A., Phoenix, G., Pomeroy, J., Rautio, A., Robinson, D., Schmidt, N., Serreze, M., Shevchenko, V., Shiklomanov, A., Shmakin, A., Sköld, P., Sturm, M., Woo, M.-k., and Wood, E.: Multiple Effects of
600   Changes in Arctic Snow Cover. Ambio, 40, 32-45, doi: 10.1007/s13280-011-0213-x, 2011a.

Callaghan, T., Tweedie, C., Akerman, J., Andrews, C., Bergstedt, J., Butler, M., Christensen, T., Cooley, D., Dahlberg, U., Danby, R., Daniëls, F., de Molenaar, J., Dick, J., Mortensen, C. E., Ebert-May, D., Emanuelsson, U., Eriksson, H., Hedenås, H., Henry, G., Hik, D., Hobbie, J., Jantze, E., Jaspers, C., Johansson, C., Johansson,
605   M., Johnson, D., Johnstone, J., Jonasson, C., Kennedy, C., Kenney, A., Keuper, F., Koh, S., Krebs, C., Lantuit, H., Lara, M., Lin, D., Lougheed, V., Madsen, J., Matveyeva, N., McEwen, D., Myers-Smith, I., Narozhniy, Y., Olsson, H., Pohjola, V., Price, L., Rigét, F., Rundqvist, S., Sandström, A., Tamstorf, M., Bogaert, R. V., Villarreal, S., Webber, P., and Zemtsov, V.: Multi-Decadal Changes in Tundra Environments and Ecosystems: Synthesis of the International Polar Year-Back to the Future Project (IPY-BTF). Ambio, 40(6), 705-716, doi:
610   10.1007/s13280-011-0179-8, 2011b.

Canadian Forest Inventory Committee (CFI): Canada's National Forest Inventory ground sampling guidelines: specifications for ongoing measurement. Pacific Forestry Centre, Victoria, British Columbia, Canada, Catalog ID 29402, ISBN 978-1-100-11329-6, 271 pages, 2008.

615

Carreiras, J., Quegan, S., Le Toan, T., Ho Tong Minh, D., Saatchi, S., Carvalhais, N., Reichstein, M., and Scipal, K.: Coverage of high biomass forests by the ESA BIOMASS mission under defense restrictions. Remote Sens. Environ., 196, 154-162, doi: 10.1016/j.rse.2017.05.003, 2017.

620   Christiansen, C., Schmidt, N., and Michelsen, A.: High Arctic dry heath CO_2 exchange during the early cold season. Ecosystems, 15(7), 1083–1092, doi: 10.1007/s10021-012-9569-4, 2012.

Davidson, E., and Janssens, I.: Temperature sensitivity of soil carbon decomposition and feedbacks to climate change. Nature, 440, 165–173, doi:10.1038/nature04514, 2006.

625

Derksen, C., Burgess, D., Duguay, C., Howell, S., Mudryk, L., Smith, S., Thackeray, C., and Kirchmeier-Young, M.: Changes in snow, ice, and permafrost across Canada. Canada's Changing Climate Report – Chapter 5, Government of Canada, Ottawa, Ontario, Canada, 194–260, 2019.

630   Devoie, É., Gruber, S., and McKenzie, J.: A repository of measured soil freezing characteristic curves: 1921 to 2021. Earth Syst. Sci. Data, 14(7), 3365-3377, doi: 10.5194/essd-14-3365-2022, 2022.

Dominé, F., Barrère, M., Sarrazin, D., Morin, S., and Arnaud, L.: Automatic monitoring of the effective thermal conductivity of snow in a low-Arctic shrub tundra. Cryosphere, 9(3), 1265-1276, doi: 10.5194/tc-9-1265-2015, 635   2015.

Dominé, F., Barrère, M., and Sarrazin, D. : Seasonal evolution of the effective thermal conductivity of the snow and the soil in high Arctic herb tundra at Bylot Island, Canada. Cryosphere, 10, 2573-2588, doi: 10.5194/tc-10-2573-2016, 2016a.
640

Dominé, F., Barrère, M., and Morin, S.: The growth of shrubs on high Arctic tundra at Bylot Island: Impact on snow physical properties and permafrost thermal regime. Biogeosciences, 13(23), 6471-6486, doi: 10.5194/bg-13-6471-2016, 2016b.

645   Dominé, F., Fourteau, K., Picard, G., Lackner, G., Sarrazin, D., and Poirier, M.: Permafrost cooled in winter by thermal bridging through snow-covered shrub branches. Nat. Geosci., 15, 554-560, doi: 10.1038/s41561-022-00979-2, 2022.

Elberling, B.: Annual soil CO_2 effluxes in the High Arctic: The role of snow thickness and vegetation type. Soil Biol. 650   Biochem., 39(2), 646-654, doi: 10.1016/j.soilbio.2006.09.017, 2007.

Fierz, C., R. L., A., Durand, Y., Etchevers, P., Green, E., McClung, D., Nishimura, K., Satyawali, P., and Sokratov, S.: The International Classification for Seasonal Snow on the Ground, IHP-VII Technical Documents in Hydrology N83, IACS Contribution N1, UNESCO-IHP, Paris, 2009.
655

Fisher, J., Sikka, M., Oechel, W., Huntzinger, D., Melton, J., Koven, C., Ahlström, A., Arain, M., Baker, I., Chen, J., Ciais, P., Davidson, C., Dietze, M., El-Masri, B., Hayes, D., Huntingford, C., Jain, A., Levy, P., Lomas, R., Poulter, B., Price, D., Sahoo, A., Schaefer, K., Tian, H., Tomelleri, E., Verbeeck, H., Viovy, N., Wania, R., Zeng, N., and Miller, C.: Carbon cycle uncertainty in the Alaskan Arctic. Biogeosciences, 11(15), 4271-4288, 660   doi: 10.5194/bg-11-4271-2014, 2014.

Fisher, J., Sikka, M., Block, G., Schwalm, C., Parazoo, N., Kolus, H., Sok, M., Wang, A., Gagne-Landmann, A., Lawal, S., Guillaume, A., Poletti, A., Schaefer, K., El Masri, B., Levy, P., Wei, Y., Dietze, M., and Huntzinger, D.: The Terrestrial Biosphere Model Farm. J. Adv. Model Earth Syst., 14(2), e2021MS002676, doi: 665   10.1029/2021MS002676, 2022.

Fooladmand, H. R.: Estimating soil specific surface area using the summation of the number of spherical particles and geometric mean particle-size diameter. Afr. J. Agric. Res., 6(7), 1758-1762, doi: 10.5897/AJAR11.19, 2011.

670   Gauthier, S., Bernier, P., Kuuluvainen, T., Shvidenko, A., and Schepaschenko, D.: Boreal forest health and global change. Science, 349(6250), 819-822, doi: 10.1126/science.aaa9092, 2015.

Gouttevin, I., Menegoz, M., Dominé, F., Krinner, G., Koven, C., Ciais, P., Tarnocai, C., and Boike, J.: How the insulating properties of snow affect soil carbon distribution in the continental pan-Arctic area. Biogeosciences, 117(G2), G02020, doi: 10.1029/2011JG001916, 2012.

Graham, L., and Risk, D.: Explaining CO2 fluctuations observed in snowpacks. Biogeosciences, 15(3), 847–859, doi:10.5194/bg-15-847-2018. 2018.

Grünberg, I., Wilcox, E., Zwieback, S., Marsh, P., and Boike, J.: Linking tundra vegetation, snow, soil temperature, and permafrost. Biogeosciences, 17(16), 4261-4279, doi: 10.5194/bg-17-4261-2020, 2020.

Harel, A., Sylvain, J., Drolet, G., Thiffault, E., Thiffault, N., and Tremblay, S.: Fine scale assessment of seasonal, intra-seasonal and spatial dynamics of soil CO2 effluxes over a balsam fir-dominated perhumid boreal landscape. Agric. For. Meteorol., 335, 109469, doi: 10.1016/j.agrformet.2023.109469, 2023.

Harvey, A., In Haynes, W., Lide, D., and Bruno, T.: CRC Handbook of Chemistry and Physics (97th ed.): Properties of Ice and Supercooled Water. CRC Press, Boca Raton, Florida, United States, 2666 pages (6-12). ISBN 978-1-4987-5429-3, 2017.

Hayes, J., McGuire, A., Kicklighter, D., Gurney, K., Burnside, T., and Melillo, J.: Is the northern high-latitude land-based CO2 sink weakening?. Glob. Biogeochem. Cycles, 25(3), GB3018, doi: 10.1029/2010GB003813, 2011.

van Huissteden, J., and Dolman, A.: Soil carbon in the Arctic and the permafrost carbon feedback. Current Opinion in Environmental Sustainability, 4(5), 545-551, doi: 10.1016/j.cosust.2012.09.008, 2012.

Jentzsch, K., Boike, J., and Foken, T.: Importance of the Webb, Pearman, and Leuning (WPL) correction for the measurement of small CO2 fluxes. Atmos. Meas. Tech., 14(11), 7291-7296, doi: 10.5194/amt-14-7291-2021, 2021.

Jones, H., Pomeroy, J., Davies, T., Tranter, M., and Marsh, P.: CO_2 in Arctic snow cover: landscape form, in-pack gas concentration gradients, and the implications for the estimation of gaseous fluxes. Hydrol. Process., 13-18, 2977-2989, doi: 10.1002/(SICI)1099-1085(19991230)13:18<2977::AID-HYP12>3.0.CO;2-%23, 1999.

Kibtia, H., Abdullah, S., and Bustamam, A.: Comparison of random forest and support vector machine for prediction of cognitive impairment in Parkinson's disease. AIP Conf. Proc., 2296(1), 020093, doi: 10.1063/5.0030332, 2020.

Kim, Y., Tsunogai, S., and Tanaka, N.: Winter CO_2 emission and its production rate in cold temperate soils of northern Japan: ^{222}Rn as a proxy for the validation of CO_2 diffusivity. Polar Sci., 22, 100480, doi: 10.1016/j.polar.2019.09.002, 2019.

Kinar, N., and Pomeroy, J.: Measurement of the physical properties of the snowpack. Rev. Geophys., 53(2), 481-544, doi: 10.1002/2015RG00048, 2015.

715 Knowles, J., Blanken, P., and Williams, M.: Soil respiration variability across a soil moisture and vegetation community gradient within a snow-scoured alpine meadow. Biogeochemistry 125, 185–202, doi: 10.1007/s10533-015-0122-3, 2015.

Krogh, S., Pomeroy, J., and Marsh, P.: Diagnosis of the hydrology of a small Arctic basin at the tundra-taiga transition
720 using a physically based hydrological model. J. Hydrol., 550, 685-703, doi: 10.1016/j.jhydrol.2017.05.042, 2017.

Kropp, H., Loranty, M., Rutter, N., Fletcher, C., Derksen, C., Mudryk, L., and Todt, M.: Are vegetation influences on Arctic–boreal snow melt rates detectable across the Northern Hemisphere?. Environ. Res. Lett., 17, 104010,
725 doi: 10.1088/1748-9326/ac8fa7, 2022.

Lawrence, D., Fisher, R., Koven, C., Oleson, K., Swenson, S., Bonan, G., Collier, N., Ghimire, B., Kampenhout, L., Kennedy, D., Kluzek, E., Lawrence, P., Li, F., Li, H., Lombardozzi, D., Riley, W., Sacks, W., Shi, M., Vertenstein, M., Wieder, W., Xu, C., Ali, A., Badger, A., Bisht, G., Broeke, M., Brunke, M., Burns, S., Buzan,
730 J., Clark, M., Craig, A., Dahlin, K., Drewniak, B., Fisher, J., Flanner, M., Fox, A., Gentine, P., Hoffman, F., Keppel-Aleks, G., Knox, R., Kumar, S., Lenaerts, J., Leung, L. R., Lipscomb, W., Lu, Y., Pandey, A., Pelletier, J., Perket, J., Randerson, J., Ricciuto, D., Sanderson, B., Slater, A., Subin, Z., Tang, J., Thomas, R. Q., Val Martin, M., and Zeng, X.: The Community Land Model version 5: Description of new features, benchmarking, and impact of forcing uncertainty. J. Adv. Model. Earth Syst., 11(12, 4245-4287, doi:10.1029/2018MS001583,
735 2019.

Liaw, A., and Wiener, M.: Classification and Regression by Randomforest. R News, 2(3), 18-22, 2002.

Linn, D., and Doran, J.: Effect of Water Filled Pore Space on Carbon Dioxide and Nitrous Oxide Production in Tilled
740 and Non-Tilled Soils. Soil Sci. Soc. Am. J., 48(6), 1267-1272, doi: 10.2136/sssaj1984.03615995004800060013x, 1984.

Loranty, M., Abbott, B., Blok, D., Douglas, T., Epstein, H., Forbes, B., Jones, B., Kholodov, A., Kropp, H., Malhotra, A., Mamet, S., Myers-Smith, I., Natali, S., O'Donnell, J., Phoenix, G., Rocha, A., Sonnentag, O., Tape, K., and
745 Walker, D.: Reviews and syntheses: Changing ecosystem influences on soil thermal regimes in northern high-latitude permafrost regions. Biogeosciences, 15(17), 5287–5313, doi:10.5194/bg-15-5287-2018, 2018.

Maier, M., Weber, T., Fiedler, J., Fuß, R., Glatzel, S., Huth, V., Jordan, S., Jurasinski, G., Kutzbach, L., Schäfer, K., Weymann, D., and Hagemann, U.: Introduction of a guideline for measurements of greenhouse gas fluxes
750 from soils using non-steady-state chambers. J. Soil Sci. Plant Nutr., 185(4), 447-461, doi: 10.1002/jpln.202200199, 2022.

Marrero, T., and Mason E.: Gaseous diffusion coeffcients. J. Phys. Chem. Ref. Data, 1(1), 3-117, doi: 10.1063/1.3253094, 1972.
755

Martin, M., Kumar, P., Sonnentag, O., and Marsh, P.: Thermodynamic basis for the demarcation of Arctic and alpine treelines. Sci. Rep., 12, 12565, doi: 10.1038/s41598-022-16462-2, 2022.

760 Massman, W.: A review of the molecular diffusivities of H_2O, CO_2, CH_4, CO, O_3, SO_2, NH_3, N_2O, NO, and NO_2 in air, O_2 and N_2 near STP. Atmos. Environ., 32(6), 1111-1127, doi: 10.1016/S1352-2310(97)00391-9, 1998.

Mast, M. A., Wickland, K., Striegl, R., and Clow, D.: Winter fluxes of CO_2 and CH_4 from subalpine soils in Rocky Mountain National Park, Colorado. Glob. Biogeochem. Cycles, 12(4), 607-620, doi: 10.1029/98GB02313, 1998.

765

McDowell, N., Marshall, J., Hooker, T., and Musselman, R.: Estimating CO2 flux from snowpacks at three sites in the Rocky Mountains. Tree physiol., 20(11), 745–753, doi: 10.1093/treephys/20.11.745, 2000.

McMahon, S., Parker, G., and Miller, D.: Evidence for a recent increase in forest growth. Proc. Natl. Acad. Sci. U.S.A., 770 107(8), 3611-3615, doi: 10.1073/pnas.0912376107, 2010.

Mellander, P., Löfvenius, M., and Laudon, H.: Climate change impact on snow and soil temperature in boreal Scots pine stands. Clim. Change, 85, 179–193, doi:10.1007/s10584-007-9254-3, 2007.

775 Meloche, J., Langlois, A., Rutter, N., McLennan, D., Royer, A., Billecocq, P., and Ponomarenko, S.: High-resolution snow depth prediction using Random Forest algorithm with topographic parameters: A case study in the Greiner watershed, Nunavut. Hydrol. Process., 36(3), e14546, doi: 10.1002/hyp.14546, 2021.

Melton, J., Arora, V., Wisernig-Cojoc, E., Seiler, C., Fortier, M., Chan, E., and Teckentrup, L.: CLASSIC v1.0: the open- 780 source community successor to the Canadian Land Surface Scheme (CLASS) and the Canadian Terrestrial Ecosystem Model (CTEM) – Part 1: Model framework and site-level performance. Geosci. Model Dev., 13(6), 2825-2850, doi: 10.5194/gmd-13-2825-2020, 2020.

Ménard, C., Essery, R., Pomeroy, J., Marsh, P., and Clark, D.: A shrub bending model tocalculate the albedo of shrub- 785 tundra. Hydrol. Process., 28(2), 341-351, doi: 10.1002/hyp.9582, 2012.

Michaelson, G. J., and Ping, C. L.: Soil organic carbon and CO2 respiration at subzero temperature in soils of Arctic Alaska. J. Geophys. Res. Atmos. 108(D2), 8164, doi: 10.1029/2001JD000920, 2005.

790 Millington, R. J.: Gas Diffusion in Porous Media. Science, 130(3367), 100-102, doi: 10.1126/science.130.3367.100-a, 1959.

Miner, K., Turetsky, M., Malina, E., Bartsch, A., Tamminen, J., McGuire, A. D., Fix, A., Sweeney, C., Elder, C., and Miller, C.: Permafrost carbon emissions in a changing Arctic. Nat. Rev. Earth Environ., 3, 55–67, 795 doi:10.1038/s43017-021-00230-3, 2022.

Monson, R., Lipson, D., Burns, S., Turnipseed, A., Delany, A., Williams, M., and Schmidt, S.: Winter forest soil respiration controlled by climate and microbial community composition. Nature, 439, 711–714, doi: 10.1038/nature04555, 2006.

800

Myers-Smith, I. H., Kerby, J., Phoenix, G., Bjerke, J., Epstein, H., Assmann, J., John, C., Andreu-Hayles, L., Angers-Blondin, S., Beck, P., Berner, L., Bhatt, U., Björkman, A., Blok, C., Bryn, A., Christiansen, C., Cornelissen, J. H. C., Cunliffe, A., Elmendorf, S., Forbes, B., Goetz, S., Hollister, R., de Jong, R., Loranty, M., Macias-Fauria, M., Maseyk, K., Normand, S., Olofsson, J., Parker, T., Parmentier, F.-J., Post. E., Schaepman-Strub, G.,

805   Stordal, F., Sullivan, P., Thomas, H., Tømmervik, H., Treharne, R., Tweedie, C., Walker, D., Wilmking, M., and Wipf, S.: Complexity revealed in the greening of the Arctic. Nat. Clim. Change, 10, 106-117, doi: 10.1038/s41558-019-0688-1, 2020.

Natali, S.,Watts, J., Rogers, B., Potter, S., Ludwig, S., Selbmann, A.-K., Sullivan, P., Abbott, B., Arndt, K., Birch, L.,

810   Björkman, M., Bloom, A., Celis, G., Christensen, T., Christiansen, C., Commane, R., Cooper, E., Crill, P., Czimczik, C., Davydov, S., Du, J., Egan, J., Elberling, B., Euskirchen, E., Friborg, T., Genet, H., Göckede, M., Goodrich, J., Grogan, P., Helbig, M., Jafarov, E., Jastrow, J., Kalhori, A., Kim, Y., Kimball, J., Kutzbach, L., Lara, M., Larsen, K., Lee, B.-Y., Liu, Z., Loranty, M., Lund, M., Lupascu, M., Madani, N., Malhotra, A., Matamala, R., McFarland, J., McGuire, A., Michelsen, A., Minions, C., Oechel, W., Olefeldt, D., Parmentier,

815   F.-J., Pirk, N., Poulter, B., Quinton, W., Rezanezhad, F., Risk, D., Sachs, T., Schaefer, K., Schmidt, N., Schuur, E., Semenchuk, P., Shaver, G., Sonnentag, O., Starr, G., Treat, C., Waldrop, M., Wang, Y., Welker, J., Wille, C., Xu, X., Zhang, Z., Zhuang, Q., and Zona, D.: Large loss of CO_2 in winter observed across the northern permafrost region. Nat. Clim. Change, 9, 852-857, doi: 10.1038/s41558-019-0592-8, 2019.

820 Natali, S., Holdren, J., Rogers, B., Treharne, R., Duffy, P., Pomerance, R., and MacDonald, E.: Permafrost carbon feedbacks threaten global climate goals. Proc. Natl. Acad. Sci. U.S.A., 118(21), e2100163118, doi: 10.1073/pnas.2100163118, 2021.

Outcalt, S., Nelson, F., and Hinkel, K.: The zero-curtain effect: Heat and mass transfer across an isothermal region in

825   freezing soil. Water Resour. Res., 26(7), 1509-1516, doi: 10.1029/WR026i007p01509, 1990.

Pallandt, M., Kumar, J., Mauritz, M., Schuur, E., Virkkala, A.-M., Celis, G., Hoffman, F., and Göckede, M.: Representativeness assessment of the pan-Arctic eddy-covariance site network, and optimized future enhancements. Biogeosciences, 19(3), 559-583, doi: 10.5194/bg-19-559-2022, 2022.

830

Pastorello, G., Trotta, C., Canfora, E., et al.: The FLUXNET2015 dataset and the ONEFlux processing pipeline for eddy covariance data. Sci. Data, 7, 225, doi: 10.1038/s41597-020-0534-3, 2020.

Pedron, S., Jespersen, R., Xu, X., Khazindar, Y., Welker, J., and Czimczik, C.: More Snow Accelerates Legacy Carbon

835   Emissions From Arctic Permafrost. AGU adv., 4(4), e2023AV000942, doi: 10.1029/2023AV000942, 2023.

Pirk, N., Santos, T., Gustafson, C., Johansson, A., Tufvesson, F., Tamstorf, Parmentier, F.-J., Mastepanov, M., and Christensen, T.: Methane emission bursts from permafrost environments during autumn freeze-in: New insights

from ground-penetrating radar. Geophysical Research Letters, 42(16), 6732-6738, doi: 10.1002/2015GL065034, 2015.

Pirk, N., Tamstorf, M., Lund, M., Mastepanov, M., Pedersen, S., Myllus, M., Parmentier, F.-J., Christiansen, H., and Christensen, T.: Snowpack fluxes of methane and carbon dioxide from high Arctic tundra. Biogeosciences, 121(11), 2886-2900, doi: 10.1002/2016JG003486, 2016.

Ponomarenko, S., McLennan, D., Pouliot, D., and Wagner, J.: High Resolution Mapping of Tundra Ecosystems on Victoria Island, Nunavut – Application of a Standardized Terrestrial Ecosystem Classification. Can. J. Remote., 45(5), 551-571, doi: 10.1080/07038992.2019.1682980, 2019.

Potapov, P., Hansen, M., Stehman, S., Loveland, T., and Pittman, K.: Combining MODIS and Landsat imagery to estimate and map boreal forest cover loss. Remote Sens Environ., 112(9), 3708-3719, doi: 10.1016/j.rse.2008.05.006, 2008.

Du Plessis, P., and Masliyah, J.: Flow through isotropic granular porous media. Transp. Porous Media, 6(3), 207–221, doi: 10.1007/BF00208950, 1991.

Prince, M., Roy, A., Royer, A., and Langlois, A.: Timing and spatial variability of fall soil freezing in boreal forest and its effect on SMAP L-band radiometer measurements. Remote Sens Environ., 231(9), 111230, doi: 10.1016/j.rse.2019.111230, 2019.

Proksch, M., Rutter, N., Fierz, C., and Schneebeli, M.: Intercomparison of snow density measurements: bias, precision, and vertical resolution. Cryosphere, 10(1), 371-384, doi: 10.5194/tc-10-371-2016, 2016.

Rantanen, M., Karpechko, A.Y., Lipponen, A., Nordling, K., Hyvärinen, O., Ruosteenoja, K., Vihma, T. and Laaksonen, A.: The Arctic has warmed nearly four times faster than the globe since 1979. Commun. Earth Environ., 3(1), 1-10, doi: 10.1038/s43247-022-00498-3, 2022.

Ravn, N., Elberling, B., and Michelsen, A.: Arctic soil carbon turnover controlled by experimental snow addition, summer warming and shrub removal. Soil Biol. Biochem., 142, 107698, doi: 10.1016/j.soilbio.2019.107698, 2020.

Royer, A., Dominé, F., Roy, A., Langlois, A., Marchand, N., and Davesne, G.: New northern snowpack classification linked to vegetation cover on a latitudinal mega-transect across northeastern Canada. Écoscience, 28(3-4), 225-242, doi: 10.1080/11956860.2021.1898775, 2021.

Schuur, E., McGuire, A., Schädel, C., Grosse, G., Harden, J., Hayes, D., Hugelius, G., Koven, C., Kuhry, P., Lawrence, D., Natali, S., Olefeldt, D., Romanovsky, V., Schaefer, K., Turetsky, M., Treat, C., and Vonk, J.: Climate change and the permafrost carbon feedback. Nature, 520, 171-179, doi: 10.1038/nature14338, 2015.

880 Seiler, C., Melton, J., Arora, V., and Wang, L.: CLASSIC v1.0: the open-source community successor to the Canadian Land Surface Scheme (CLASS) and the Canadian Terrestrial Ecosystem Model (CTEM) – Part 2: Global benchmarking. Geosci. Model Dev., 14(5), 2371-2417, doi: 10.5194/gmd-14-2371-2021, 2021.

Seok,B., Helmig, D., Williams, M., Liptzin, D., Chowanski, K., and Hueber, J.: An automated system for continuous
885 measurements of trace gas fluxes through snow: an evaluation of the gas diffusion method at a subalpine forest site, Niwot Ridge, Colorado. Biogeochemistry, 95, 95-113, doi: 10.1007/s10533-009-9302-3, 2009.

Slater, A., Lawrence, D., and Koven, C.: Process-level model evaluation: a snow and heat transfer metric. Cryosphere, 11(2), 989–996, doi: 10.5194/tc-11-989-2017, 2017.
890

Sommerfeld, R., Mosier, A., and Musselman, R.: CO_2, CH_4 and N_2O flux through a Wyoming snowpack and implications for global budgets. Nature, 361, 140-142, doi: 10.1038/361140a0, 1993.

Sommerfeld, R., Massman, W., Musselman, R., and Mosier., A.: Diffusional flux of CO_2 through snow : spatial and
895 temporal variability among alpine–subalpine sites. Global Biogeochem. Cycles, 10(3), 473–482, doi: 10.1029/96GB01610, 1996.

Steponavičienė, V., Bogužas, V., Sinkevičienė, A., Skinulienė, L., Vaisvalavičius, R., and Sinkevičius, A.: Soil Water Capacity, Pore Size Distribution, and CO2 Emission in Different Soil Tillage Systems and Straw Retention.
900 Plants, 11(5), 614, doi: 10.3390/plants11050614, 2022.

Strobl, C., Boulesteix, A.-L., Kneib, T., Augustin, T., and Zeileis, A.: Conditional variable importance for random forests. BMC Bioinform., 9(1), 307, doi: 10.1186/1471-2105-9-307, 2008.

905 Sturm, M., Schimel, J., Michaelson, G., Welker, J., Oberbauer, S., Liston, G., Fahnestock, J., and Romanovsky, V.: Winter biological processes could help convert arctic tundra to shrubland. Bioscience, 55, 17–26, doi: 10.1641/0006-3568(2005)055[0017:WBPCHC]2.0.CO;2, 2005.

Subke, J., Kutzbach, L., and Risk, D.: Soil Chamber Measurements. In: Springer Handbook of Atmospheric
910 Measurements. Springer Nature Switzerland AG, Cham, Switzerland, 1806 pages, doi: 10.1007/978-3-030-52171-4_60, 2021.

Tao, J., Zhu, Q., Riley, W., and Neumann, R.: Improved ELMv1-ECA Simulations of Zero-Curtain Periods and Cold-season CH_4 and CO_2 Emissions at Alaskan Arctic Tundra Sites. Cryosphere, 15(12), 5281-5307, doi:
915 10.5194/tc-2020-262, 2020.

Tarnocai, C., Canadell, J., Schuur, E., Kuhry, P., Mazhitova, G., and Zimov, S.: Soil organic carbon pools in the northern circumpolar permafrost region. Global Biogeochem. Cycles, 23(2), GB2023, doi: 10.1029/2008GB003327, 2009.
920

Taylor, J.R.: An Introduction to Error Analysis: The Study of Uncertainties in Physical Measurements. 2nd Edition, University Science Books, Sausalito, United States, 343 pages, ISBN-10: 093570275X, 1997.

Tei, S., and Sugimoto, A.: Excessive positive response of model-simulated land net primary production to climate changes over circumboreal forests. Plant-Environment Interactions, 1(2), 102-121, doi: 10.1002/pei3.10025, 2020.

Throop, J., Lewkowicz, A., and Smith, S.: Climate and ground temperature relations at sites across the continuous and discontinuous permafrost zones, northern Canada. Can. J. Earth Sci., 49(8), 865-876, doi: 10.1139/e11-075, 2012.

Virkkala, A.-M., Aalto, J., Rogers, B., Tagesson, T., Treat, C., Natali, S., Watts, J., Potter, S., Lehtonen, A., Mauritz, M., Schuur, E., Kochendorfer, J., Zona, D., Oechel, W., Kobayashi, H., Humphreys, E., Goeckede, M., Iwata, H., Lafleur, P., Euskirchen, E., Bokhorst, S., Marushchak, M., Martikainen, P., Elberling, B., Voigt, C., Biasi, C., Sonnentag, O., Parmentier, F.-J., Ueyama, M., Celis, G., St.Louis, V., Emmerton, C., Peichl, M., Chi, J., Järveoja, J., Nilsson, M., Oberbauer, S., Torn, M., Park, S.-J., Dolman, H., Mammarella, I., Chae, N., Poyatos, R., López-Blanco, E., Christensen, T., Kwon, M., Sachs, T., Holl, D., and Luoto, M.: Statistical upscaling of ecosystem CO_2 fluxes across the terrestrial tundra and boreal domain: Regional patterns and uncertainties. Glob. Chang. Biol., 27(17), 4040-4059, doi: 10.1111/gcb.15659, 2021.

Virkkala, A.-M., Natali, S., Rogers, B., Watts, J., Savage, K., Connon, S., Mauritz, M., Schuur, E., Peter, D., Minions, C., Nojeim, J., Commane, R., Emmerton, C., Goeckede, M., Helbig, M., Holl, D., Iwata, H., Kobayashi, H., Kolari, P., López-Blanco, E., Marushchak, M., Mastepanov, M., Merbold, L., Parmentier, F.-J., Peichl, M., Sachs, T., Sonnentag, O., Ueyama, M., Voigt, C., Aurela, M., Boike, J., Celis, G., Chae, N., Christensen, T. R., Bret-Harte, M., Dengel, S., Dolman, H., Edgar, C., Elberling, B., Euskirchen, E., Grelle, A., Hatakka, J., Humphreys, E., Järveoja, J., Kotani, A., Kutzbach, L., Laurila, T., Lohila, A., Mammarella, I., Matsuura, Y., Meyer, G., Nilsson, M., Oberbauer, S., Park, S.-J., Petrov, R., Prokushkin, A., Schulze, C., St. Louis, V., Tuittila, E.-S., Tuovinen, J.-P., Quinton, W., Varlagin, A., Zona, D., and Zyryanov, V.: The ABCflux database: Arctic–boreal CO2 flux observations and ancillary information aggregated to monthly time steps across terrestrial ecosystems. Earth Syst. Sci. Data, 14(1), 179–208, doi: 10.5194/essd-14-179-2022, 2022.

Virtanen, T. and Ek, M.: The fragmented nature of tundra landscape. Int. J. Appl. Earth Obs. Geoinf., 27(A), 4-12, doi: 10.1016/j.jag.2013.05.010, 2014.

Wang, T., Ciais, P., Piao, S., Ottlé, C., Brender, P., Maignan, F., Arain, A., Cescatti, A., Gianelle, D., Gough, C., Gu, L., Lafleur, P., Laurila, T., Marcolla, B., Margolis, H., Montagnani, L., Moors, E., Saigusa, N., Vesala, T., Wohlfahrt, G., Koven, C., Black, A., Dellwik, E., Don, A., Hollinger, D., Knohl, A., Monson, R., Munger, J., Suyker, A., Varlagin, A., and Verma, S.: Controls on winter ecosystem respiration in temperate and boreal ecosystems. Biogeosciences, 8(7), 2009–2025, doi: 10.5194/bg-8-2009-2011, 2011.

Wieder, W., Sulman, B., Hartman, M., Koven, C., and Bardford, M.: Arctic Soil Governs Whether Climate Change Drives Global Losses or Gains in Soil Carbon. Geophys. Res. Lett., 46(24), 14486-14495, doi: 10.1029/2019GL085543, 2019.

965 Wilcox, E.J., Keim, D., de Jong, T., Walker, B., Sonnentag, O., Sniderhan, A.E., Mann, P. and Marsh, P.: Tundra shrub expansion may amplify permafrost thaw by advancing snowmelt timing. Arct. Sci., 5(4), 202-217, doi: 0.1139/as-2018-0028, 2019.

Webb, E., Schuur, E., Natali, S., Oken, K., Bracho, R., Krapek, J., Risk, D., and Nickerson, N.: Increased wintertime
970 CO_2 loss ass a result of sustained tundra warming. J. Geophys. Res. Biogeosci., 121(2), 249-265, doi: 10.1002/2014JG002795, 2016.

Yi, Y., Kimball, J., Rawlins, M., Moghaddam, M., and Euskirchen, E.: The role of snow cover affecting boreal-arctic soil freeze–thaw and carbon dynamics. Biogeosciences, 12(19), 5811-5829, doi: 10.5194/bg-12-5811-2015,
975 2015.

Yi, Y., Kimball, J., Chen, R., Moghaddam, M., and Miller, C.: Sensitivity of active-layer freezing process to snow cover in Arctic Alaska. Cryosphere, 13(1), 197-218, doi: 10.5194/tc-13-197-2019, 2019.

980 Yli-Halla, M., Lötjönen, T., Kekkonen, J., Virtanen, S., Marttila, H., Liimatainen, M., Saari, M., Mikkola, J., Suomela, R., and Joki-Tokola, E.: Thickness of peat influences the leaching of substances and greenhouse gas emissions from a cultivated organic soil. Sci. Total Environ., 806(1), 150499, doi: 10.1016/j.scitotenv.2021.150499, 2022.

985 Zhang, L., Zhao, T., Jiang, L., and Zhao, K.: Estimate of Phase Transition Water Content in Freeze–Thaw Process Using Microwave Radiometer. IEEE Trans. Geosci. Remote Sens., 48(12), 4248-4255, doi: 10.1109/TGRS.2010.2051158, 2010.

Zhu, C., Nakayama, M., and Inouey, H. Y.: Continuous measurement of CO_2 flux through the snowpack in a dwarf
990 bamboo ecosystem on Rishiri Island, Hokkaido, Japan. Polar Sci., 8(3), 218-231, doi: 10.1016/j.polar.2014.04.003, 2014.

995

Appendix A

1000

Table A1: Uncertainty sources on F_{CO2} and their uncertainty. [CO₂] precision was evaluated at a concentration of 400 ppm.

F_{CO2} uncertainty source	Uncertainty
[CO₂] estimate	
• LI-7810 precision	3.52 ppm (0.88 %)
• Measurement stability	3.6 ppm (0.09 %; N=169)
• Reference gas	4 ppm (1 %)
• Calibration fit	3.04 ppm (0.76 %; N=6; σ = 0.15)
• Transfer, transport and storage test	4.44 ppm (1.11 %; N=6)
Snow density (kg/m³)	9 %
d[CO₂]/dz linear regression (gC/m⁴)	19.4 %
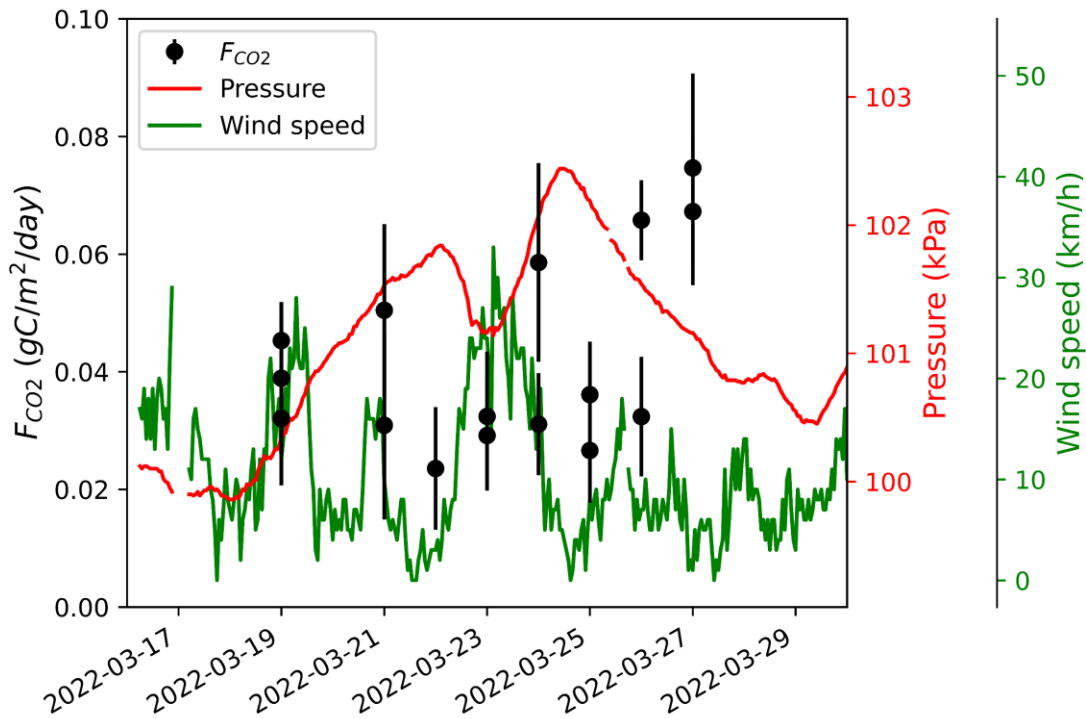
Figure A1: CO₂ fluxes (F_{CO2}) at a sampling location in the Trail Valley Creek erect-shrub tundra (lichen) between March 19th and March 27th, 2022. Atmospheric pressure and wind speed were obtained from Environment and Climate Change Canada's Meteorological Service of Canada meteorological station at Trail Valley Creek (*https://climate.weather.gc.ca/historical_data/search_historic_data_e.html*).
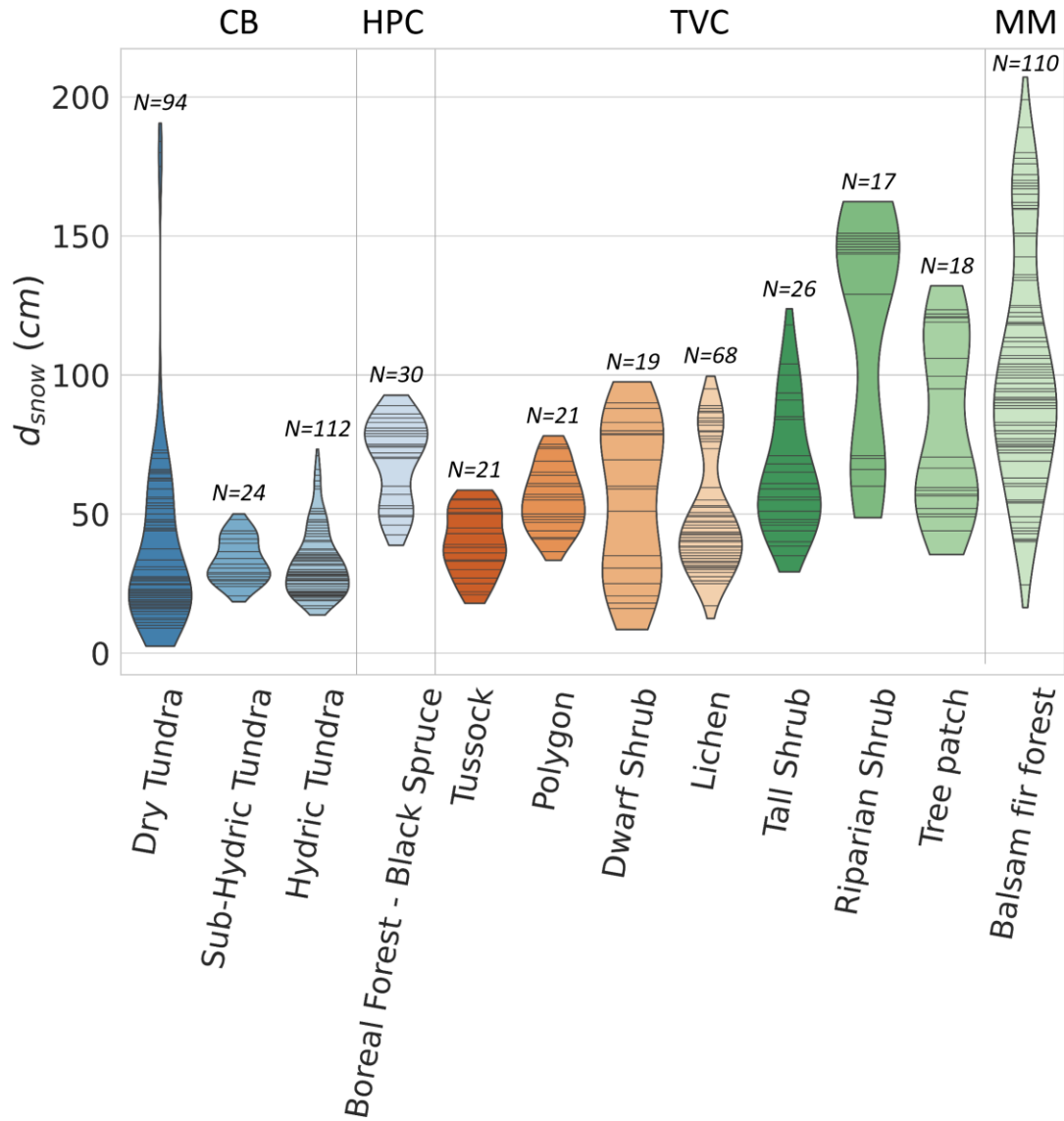
Figure A2: Violin plot of the snow depth range of sites where F_{CO_2} was estimated. The black stripes inside the violins represent data point. The study sites are Cambridge Bay (CB), Havikpak Creek (HPC), Trail Valley Creek (TVC) and Montmorency Forest (MM). CB sites are ordered by increasing hydricity and TVC sites are ordered by increasing mean soil surface temperature in March 2021 and 2022.
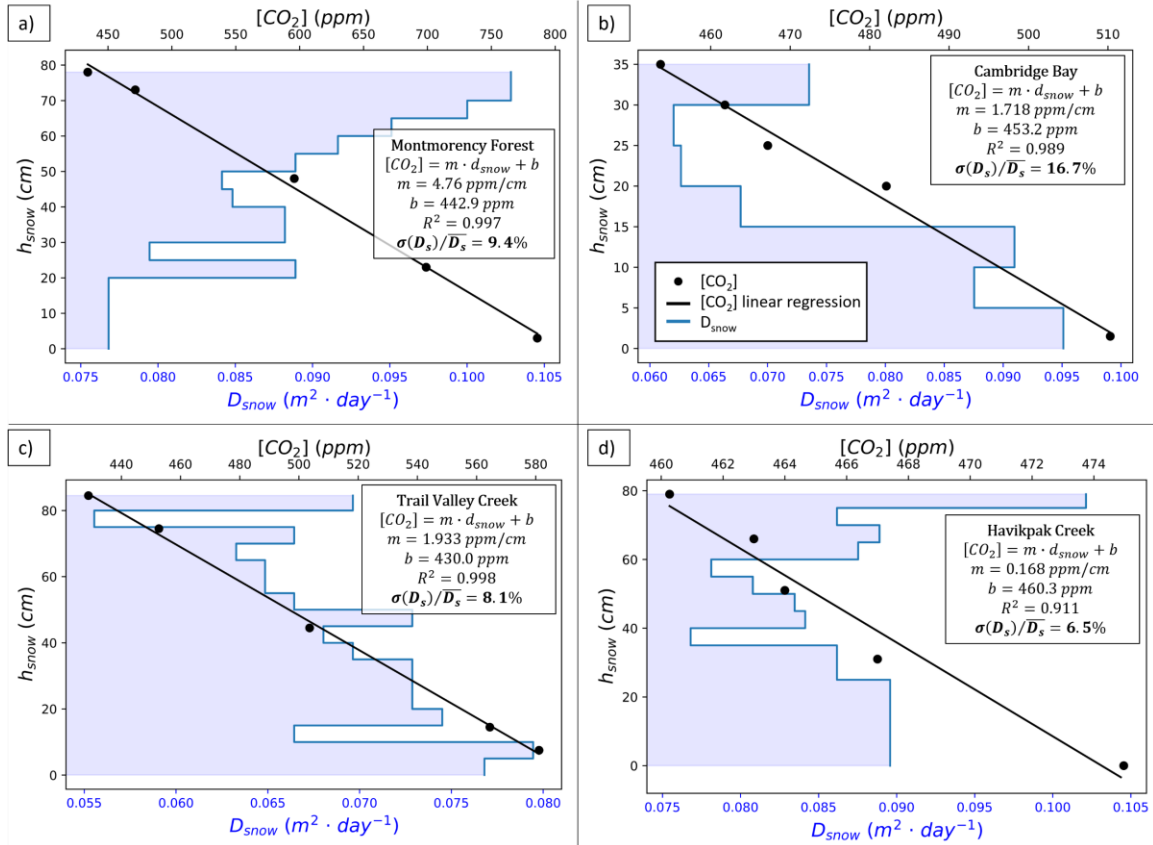
Figure A3: Examples of snow diffusion coefficient ($D_{snow} = D_{air} \cdot \varphi \cdot \tau$) vertical stratification and CO_2 concentration ([CO_2]) gradient measurements in function of snow height (h_{snow}) from the ground level. The coefficient of determination (R^2), [CO_2] gradient (m) and y-axis intercept (b) for the linear regressions on the [CO_2] gradient measurements are provided. The ratio between D_{snow} standard deviation ($\sigma(D_s)$) and average ($\overline{D_s}$) is provided in percent. The data comes from (a) Montmorency Forest balsam fir closed-crown coniferous boreal forest on 2021-02-26, (b) Cambridge Bay prostrate-shrub tundra (hydric tundra: hydric sedge fen) on 2022-04-15, (c) Trail Valley Creek erect-shrub tundra (lichen) on 2022-03-26, and (d) Havikpak Creek black spruce open-crown coniferous boreal forest on 2022-03-16.
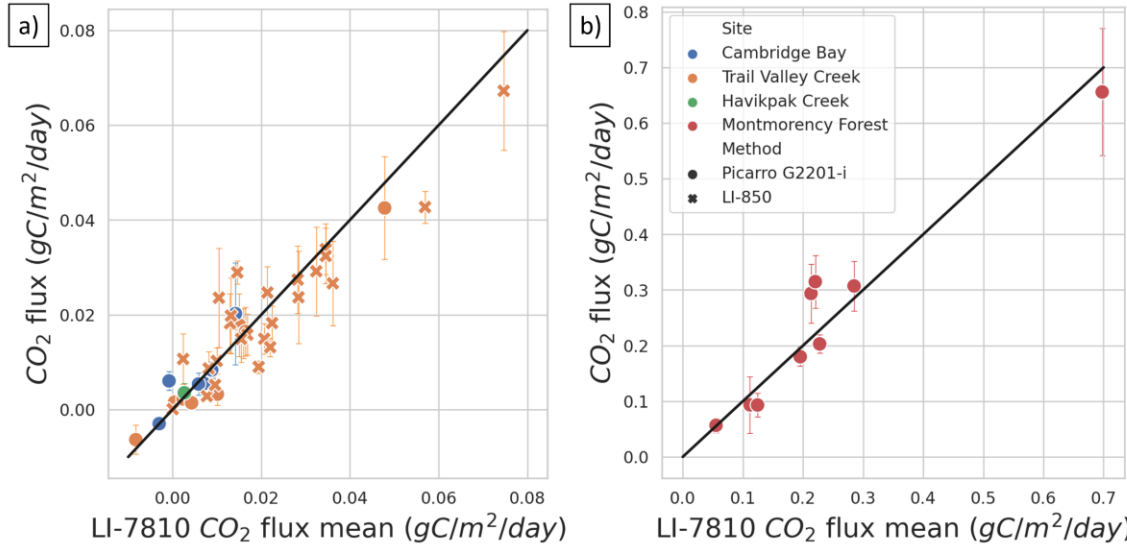
1025

Figure A4: Comparison of winter CO_2 flux calculated from CO2 concentration estimated with different gas analyzers. The LI-7810 gas analyzer was used as the reference and is compared to a Picarro G2201-*i* and LI-850. In the arctic biome (a), the correlation coefficient is 0.924 for the Picarro and 0.821 for the LI-850. In the boreal biome (b), the correlation coefficient is 0.929 for the Picarro.

1030
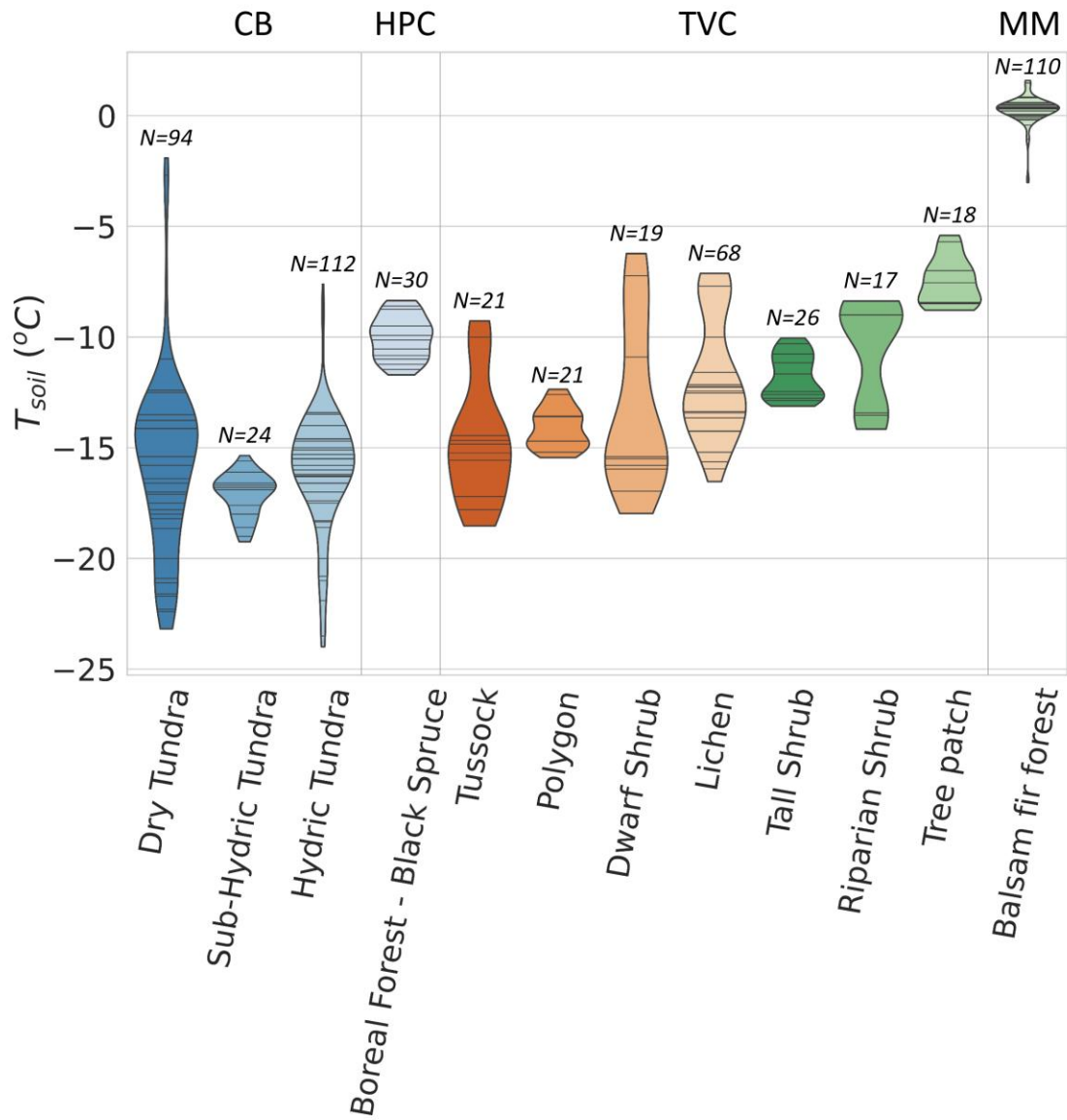
Figure A5: Violin plot of the soil temperature (T_{soil}) range of sites where F_{CO2} was estimated. The black stripes inside the violins represent data point. CB sites are ordered by increasing hygricity and TVC sites are ordered by increasing soil surface temperature in March 2021 and 2022.

1035